

N 7 1 - 2 0 4 7 2

NASA TECHNICAL
MEMORANDUM

NASA TM X-64571

CONTRIBUTIONS TO X-RAY PHYSICS IN SPACE

By Klaus Schocken
Space Sciences Laboratory

January 27, 1971

CASE FILE
COPY

NASA

*George C. Marshall Space Flight Center
Marshall Space Flight Center, Alabama*

1. REPORT NO. NASA TM X-64571		2. GOVERNMENT ACCESSION NO.		3. RECIPIENT'S CATALOG NO.	
4. TITLE AND SUBTITLE Contributions to X-Ray Physics in Space				5. REPORT DATE January 27, 1971	
				6. PERFORMING ORGANIZATION CODE	
7. AUTHOR(S) Klaus Schocken				8. PERFORMING ORGANIZATION REPORT #	
9. PERFORMING ORGANIZATION NAME AND ADDRESS George C. Marshall Space Flight Center Marshall Space Flight Center, Alabama 35812				10. WORK UNIT NO.	
				11. CONTRACT OR GRANT NO.	
12. SPONSORING AGENCY NAME AND ADDRESS National Aeronautics and Space Administration Washington, D. C. 20546				13. TYPE OF REPORT & PERIOD COVERED Technical Memorandum	
				14. SPONSORING AGENCY CODE	
15. SUPPLEMENTARY NOTES Prepared by Space Sciences Laboratory, Science and Engineering					
16. ABSTRACT <p>The first section of this report is a discussion of the continuous X-radiation in space that can originate as blackbody radiation, deceleration radiation, and by inverse Compton processes.</p> <p>It is shown that the radiation in Tau X-1 originates as synchrotron radiation, in Cyg X-2 and Sco X-1 as deceleration radiation, and the diffuse background radiation by inverse Compton processes.</p> <p>A statistical argument is presented to clarify the origin of the unidentified sources.</p> <p>In the second section the hypothesis is made that the background X-ray flux in the galaxy consists partly of synchrotron X rays that are generated in a galactic dynamo. Synchrotron radiation from the galaxy has been observed at radio frequencies. The radio emission of the galaxy provides evidence that magnetic fields extend far beyond the boundaries of the galaxy proper into a corona which is called the halo. The magnetic field of a cosmic dynamo is maintained by the induction effect of the turbulence in an electrically conducting fluid. It is probable that turbulence exists in the halo, and therefore, the existence of a dynamo in the halo is also probable.</p> <p>The last section discusses maintenance of the synchrotron radiation of the Crab Nebula by magnetic fields. The only theory that appears to be capable of accounting for the required fields is the dynamo theory. The continuum of the Crab Nebula presents a turbulent electromagnetic</p>					
17. KEY WORDS Background X Ray Crab Nebula Cygmus X-2 Scorpius X-1 Taurus X-1 Halo			18. DISTRIBUTION STATEMENT ANNOUNCE IN STAR <i>K. Schocken</i>		
19. SECURITY CLASSIF. (of this report) Unclassified		20. SECURITY CLASSIF. (of this page) Unclassified		21. NO. OF PAGES 63	22. PRICE \$3.00

ABSTRACT (Concluded)

field, and therefore, the conditions for a migratory dynamo exist. Currently, the Steenbeck and Krause model offers the best developed procedure to obtain magnetic fields by dynamo action. In this model, computer application becomes possible. It deals with the restricted problem, in which the velocity is considered as given. If a model of the Crab Nebula were known with a precision comparable to that of solar models, the structure of the magnetic field of the Crab Nebula could be computed. The radio and optical pulsar NP 0532 is also an X-ray pulsar close to the center of the Crab Nebula. It was shown that the principal properties of pulsars can be explained if the falling core of a collapsing star rebounds at finite or infinite density as assumed in the oscillating model of the universe.

TABLE OF CONTENTS

	Page
SUMMARY	1
X-RAY ASTROPHYSICS	2
Introduction	2
Identified X-Ray Sources	4
Unidentified X-Ray Sources	18
Discussion of the Results	19
THE BACKGROUND X-RAY FLUX IN THE GALAXY	28
Introduction	28
The Background X-Ray Flux	29
The Dynamo Theory of Galactic Magnetic Fields	31
Summary	33
FLUID MAGNETIC DYNAMO MODEL OF THE CRAB NEBULA	35
Introduction	35
The Crab Nebula	35
Magnetofluid Dynamos	39
The Bouncing Core Theory of the Crab's Pulsar	44
REFERENCES	47
BIBLIOGRAPHY	50

LIST OF ILLUSTRATIONS

Figure	Title	Page
1.	Schematic representation of light curve of type I supernova	24
2.	Schematic light curve of supernova of type II	25
3.	Equipotential curves of the Roche model in the orbital plane	27

LIST OF TABLES

Table	Title	Page
1.	X-Ray Sources	5
2.	Galactic Supernovae	10
3.	Intensities of Sco X-1 X Rays	15
4.	Time Variation of X-Ray Intensity from Cen X-2	17
5.	Correlation Coefficients	19
6.	Conversion from Conventional Units to Geometrical Units	21
7.	Types of Supernovae	23
8.	Physical Parameters in the Gas	30
9.	Three Type I Supernovae and Their Remnants	36

LIST OF SYMBOLS

A	baryon number
\vec{A}	vector potential
\vec{B}	magnetic induction
c	velocity of light
G	gravitational constant in general
g_{ik}	gravitational potentials
\vec{H}	magnetic field strength
h	Planck's constant
\vec{J}	current density
K	constant
k	Boltzmann's constant
L	radiant power
l	characteristic length
M	function of coordinates in Riemann space
N	number density
\vec{n}	normal vector
P	power
$P(\nu)$	power per unit frequency interval
p	pressure
R	invariant curvature

LIST OF SYMBOLS (Continued)

R_{ik}	tensor of curvature
R_m	magnetic Reynolds number
R_o	Rossby number
r	cylindrical coordinate
s	interval in Riemann space
T	temperature
T_{ik}	energy-momentum tensor
t	time
V	volume
\vec{v}	velocity of particles
W	radiation energy
x	Cartesian coordinate
x^i	coordinates in Riemann space
Z	atomic number
z	cylindrical coordinate
α	spectral index
Γ	violence of cyclonic fluid motions
ϵ	particle energy, photon energy
κ	angular wave number

LIST OF SYMBOLS (Concluded)

λ	cosmological constant
μ_0	permeability of empty space
ν	frequency
ρ	density
ρ_e	charge density
σ	conductivity
φ	cylindrical coordinate
Ω	characteristic angular velocity
ω	angular velocity

CONTRIBUTIONS TO X-RAY PHYSICS IN SPACE

SUMMARY

The first section of this report is a discussion of the continuous X-radiation in space that can originate as blackbody radiation, deceleration radiation, and by inverse Compton processes.

It is shown that the radiation in Tau X-1 originates as synchrotron radiation, in Cyg X-2 and Sco X-1 as deceleration radiation, and the diffuse background radiation by inverse Compton processes.

A statistical argument is presented to clarify the origin of the unidentified sources.

In the second section the hypothesis is made that the background X-ray flux in the galaxy consists partly of synchrotron X rays that are generated in a galactic dynamo. Synchrotron radiation from the galaxy has been observed at radio frequencies. The radio emission of the galaxy provides evidence that magnetic fields extend far beyond the boundaries of the galaxy proper into a corona which is called the halo. The magnetic field of a cosmic dynamo is maintained by the induction effect of the turbulence in an electrically conducting fluid. It is probable that turbulence exists in the halo, and therefore, the existence of a dynamo in the halo is also probable.

The last section discusses maintenance of the synchrotron radiation of the Crab Nebula by magnetic fields. The only theory that appears to be capable of accounting for the required fields is the dynamo theory. The continuum of the Crab Nebula presents a turbulent electromagnetic field, and therefore, the conditions for a migratory dynamo exist. Currently, the Steenbeck and Krause model offers the best developed procedure to obtain magnetic fields by dynamo action. In this model, computer application becomes possible. It deals with the restricted problem, in which the velocity is considered as given. If a model of the Crab Nebula were known with a precision comparable to that of solar models, the structure of the magnetic field of the Crab Nebula could be computed. The radio and optical pulsar NP 0532 is also an X-ray pulsar close to the center of the Crab Nebula. It was shown that the principal properties of

pulsars can be explained if the falling core of a collapsing star rebounds at finite or infinite density as assumed in the oscillating model of the universe.

X-RAY ASTROPHYSICS

Introduction

X-ray sources in space are young objects and lie in the spiral arms of the galaxy. Most of them lie within several degrees of the galactic plane. The distribution in longitude is highly unsymmetrical. The distances for the X-ray sources are large, of the order of $3.084 \cdot 10^{19}$ m. Closer objects would be expected to show a larger dispersion in latitude and more symmetry in longitude.

Continuous X-radiation can originate as blackbody radiation, synchrotron radiation, deceleration radiation, and by inverse Compton processes.

Blackbody radiation is characterized by the Planck distribution curve and by very high surface emissivity. It implies sources of small physical area, small angular dimensions, and lifetimes too short to be acceptable for any great number.

Synchrotron radiation is emitted by electrons moving in magnetic fields. Very high electron energies are required to produce high-energy photons by this process.

Deceleration radiation or free-free emission is generated in the interaction of charged particles with matter. It results from e-p Coulomb scattering at nonrelativistic energies and from both e-p and e-e scatterings at relativistic energies.

In the Compton scattering of a low-energy thermal photon by a high-energy electron, a high-energy scattered photon is produced with the energy being transferred from the electron.

Lines cannot be expected, except possibly for iron, and will not be considered.

The following three spectral forms have to be considered:

1. For blackbody radiation, Planck's law:

$$S(W) = C \frac{W^3}{e^{\frac{W}{kT}} - 1} .$$

2. For synchrotron or inverse Compton radiation, a power law:

$$S(W) = CW^{-\alpha} .$$

3. For deceleration radiation, an exponential law:

$$S(W) = Ce^{-\frac{W}{kT}} .$$

The problem of matching observations to such spectral functions is complicated by the usual occurrence that no single temperature describes a thermal source, and no single index fully describes a synchrotron source. A conclusive proof of synchrotron emission is the detection of polarization.

The following astronomical units are used:

$$1 \text{ parsec} = 3.0856 \times 10^{16} \text{ m} ,$$

$$1 \text{ lt yr} = 9.4605 \times 10^{15} \text{ m} ,$$

$$1 \text{ parsec} = 3.2615 \text{ lt yr} = 206\,264.8 \text{ AU} ,$$

$$1 \text{ AU} = 1.49598 \times 10^{11} \text{ m} ,$$

$$1 \text{ lt yr} = 6.324 \times 10^4 \text{ AU} ,$$

$$1 \text{ tesla} = 10^4 \text{ gauss}$$

$$1 \text{ baryon} = 1/56 \text{ of Fe}^{56} = 1.659 \times 10^{-27} \text{ kg} ,$$

$$m = -2.5 \log \frac{I}{I_0} .$$

Generally, the International System of Units has been used. However, in some cases, the equations as given by the authors have been left unchanged.

Table 1 contains the X-ray sources as identified by Fujimoto et al. [1].

Identified X-Ray Sources

Tau X-1, Sco X-1, Cyg X-2, and Cen X-2 have been identified as X-ray sources. There is evidence that Cas A and Cas B are weak X-ray sources. The nature of the remaining galactic sources is not known. The presently observed X-ray sources are located in the spiral arms.

The total number of X-ray sources in the galaxy has been estimated to about 1250. The average luminosity of the known galactic X-ray sources is about 6×10^{29} W.

Tau X-1. The Crab Nebula surrounds the center of a supernova explosion which occurred in July 1054. The distance to it is $3.639 \cdot 10^{16}$ km. However, this value has been obtained on several simplifying assumptions (e.g., by ignoring the ellipsoidal form of the filamentary shell). The true distance may be $5.242 \cdot 10^{16}$ km. The angular diameter of the visible nebulosity is 5 min. The supernova which produced the nebulosity belongs to type I (Table 2). The envelope of the ellipsoidal volume is still expanding at about 1000 km sec^{-1} .

In visible light, the Crab Nebula is an amorphous mass of white gas within tangled filaments of red-glowing hydrogen. The white light spectrum is continuous and highly polarized. This polarization, in combination with the fact that when the X-ray data are plotted together with the data of the radio and optical continuum emission, the three parts of the observed spectrum indicate a single emission continuum — with a break extending from the radio to the X-ray region — is the reason for the adoption of a synchrotron model.

Tau X-1 is a powerful X-ray source and, as all known remnants of galactic supernova without an exception, is also a radio source. To produce synchrotron radio emission requires relativistic electrons with energies of the order of $1.6 \cdot 10^{-12}$ J in a magnetic field of about 10^{-8} tesla; for the optical emission, the electron energies have to be as high as $1.6 \cdot 10^{-9}$ to $1.6 \cdot 10^{-8}$ J; to produce X rays requires the electron energy spectrum to extend to $1.6 \cdot 10^{-5}$ J. In the X-ray range, from 1 to $10 \cdot 10^{-10}$ m, the observed flux is

$$L = 4 \times 10^{29} \text{ W} \quad .$$

TABLE 1. X-RAY SOURCES [1]

Source	α		δ (deg)	F ($\text{cm}^{-2} \text{sec}^{-1}$)	F ($1 \sim 10 \cdot 10^{-10} \text{ m}$)	r ($3.084 \cdot 10^{19} \text{ m}$)	Z ($3.084 \cdot 10^{19} \text{ m}$)
	h	m					
Ser XR-1	18	45	5.3	0.7	0.7	2.5	0.22
GX + 36.3	18	25	7	0.15			
L22				0.1			
Sgr XR-1	17	55	-29.2	1.6	1.5	1.7	0.046
GX 2.6	17	45	-28	0.68			
L14	17	49	-28.2	~ 0.3			
GX 3 + 1	17	4.34	-26.13	0.40			
Sgr X-1	17	44	-23.2	----			
Sgr XR-2	18	10	-17.1	1.5	1.5	1.7	0.037
L20	18	15	-18.0	0.3			
GX 13 + 1	18	10.0	-17.13	0.25			
GX 13.5	18	25	-19	0.37			
Sgr XR-3	18	24	-14.5	2.0	2.0	1.5	0
Sgr XR-4	17	56	-21.6	2.8	2.0	1.5	0.026
L18	18	07	-22.3	0.3			
L19	18	02	-21.0	0.3			
GX + 9.1	17	50	-20	0.84			
GX 9 + 1	17	59.7	-20.53	0.60			

TABLE 1. (Continued)

Source	α		δ (deg)	F ($\text{cm}^{-2} \text{sec}^{-1}$)	F ($1 \sim 10 \cdot 10^{-10} \text{ m}$)	r ($3.084 \cdot 10^{19} \text{ m}$)	z ($3.084 \cdot 10^{19} \text{ m}$)
	h	m					
Sgr XR-5 ^a	18	26	-13	0.6	0.7	2.5	0.043
GX 16.7	18	2	-12	1.25	3.0	1.2	0.031
GX 17 + 2	18	12.7	-13.8	0.55			
L21	18	16	-14.8	0.6			
Sgr XR-6	18	02	-24.9	1.0	1.0	2.1	-0.04
GX 5-1	17	58.6	-25	0.95			
L16	18	10	-27.6	0.6	3.0	1.2	-0.02
L17	18	01	-25.6	0.7			
GX + 5.2	17	55	-26	1.24			
Sco XR-1	16	15	-15.2	18.7	20	0.47	0.19
Sco X-1	16	14	-15.6	11.0			
Sco X-1	16	17.07	-15.53	19			
Sco XR-1	16	15	-15.0	21			
Sco XR-2	17	8	-36.4	1.4	2.0	1.5	0
Sco SR-2	17	15	-38.4	2.6			
Sco XR-2	17	09	-37.7	1.1			
GX - 5.6	17	20	-35	0.11			

TABLE 1. (Continued)

Source	α		δ (deg)	F ($\text{cm}^{-2} \text{sec}^{-1}$)	F ($1 \sim 10 \cdot 10^{-10} \text{ m}$)	r ($3.084 \cdot 10^{19} \text{ m}$)	z ($3.084 \cdot 10^{19} \text{ m}$)
	h	m					
Sco X-2	16	50	-39.6	-----			
Sco XR-3	17	23	-44.3	1.1	1.0	2.1	-0.18
GX - 14.1	17	0	-40	0.11			
Sco XR-4	16	25	-40	0.8	0.8	2.4	0.21
GX - 10.7	17	15	-37	0.90			
Sco XR-5 ^a	17	37	-40.4	0.7	0.7	2.5	0
L9	17	36	-35.2	0.2	1.0	2.1	-0.11
L10'	17	45	-33.7	0.15			
GX - 2.5	17	40	-32	0.4			
Sco XR-6 ^a	18	7	-35.6	0.3			
Oph XR-1	17	32	-20.7	1.3	1.3	1.9	0.24
Oph XR-2 ^a	17	14	-23.5	0.5			
Ara XR-1	17	5	-45.9	1.9	1.9	1.5	-0.08
Nor XR-1 ^a	16	24	-51	0.8	1.0	2.1	-0.04
L2	16	54	-47.0	0.3			
L3	16	49	-45.3	0.1			
Nor XR-2 ^a	15	38	-57	0.4	0.4	3.3	-0.06

TABLE 1. (Continued)

Source	α		δ (deg)	F ($\text{cm}^{-2} \text{sec}^{-1}$)	F ($1 \sim 10 \cdot 10^{-10} \text{ m}$)	r ($3.084 \cdot 10^{19} \text{ m}$)	z ($3.084 \cdot 10^{19} \text{ m}$)
	h	m					
Lup XR-1 ^a	15	2	-52	0.2	0.2	4.7	0.41
Cen XR-1 ^a	14	28	-63	0.17	0.17	5.1	-0.18
L7	16	42	-31.9	~0.15	0.7	2.5	0.38
L8	17	01	-30.5	~0.15	0.7	2.5	0.29
L12	17	49	-31.5	~0.35	1.6	1.7	0.08
L13	17	40	-29.0	-----			
GX + 48.7	19	20	14	0.19	0.5	3.0	0
GX 9 + 9	17	30	-16.6	0.25	0.3	3.9	0.59
L5 (Sco X-2)	16	51	-40.8	0.1	0.5	3.0	0.09
GX - 12.9	<16	20	<-35	0.33	0.8	2.4	0.41
Cyg XR-1 ^b	19	53	34.5	3.6	3.0	1.2	0.06
Cyg XR-1	19	57	34.5	0.9			
L23	--	--	-----	0.8			
Cyg X-1	19	56.57	35.1	0.4			
Cyg XR-2	21	43	38.8	0.8	1.0	2.1	-0.41
Cyg XR-2	21	42	38.8	1.0			
Cyg X-2	21	42.8	38.18	0.36			

TABLE 1. (Concluded)

Source	α		δ (deg)	F ($\text{cm}^{-2} \text{sec}^{-1}$)	F ($1 \sim 10 \cdot 10^{-10} \text{ m}$)	r ($3.084 \cdot 10^{19} \text{ m}$)	s ($3.084 \cdot 10^{19} \text{ m}$)
	h	m					
Cyg XR-3	19	58	40.4	0.4	0.4	3.3	0.29
Cyg X-3	20	30.87	40.93	0.13			
Cyg XR-4 ^a	21	2	42	0.3	0.3	3.9	-0.27
Cyg X-4	21	9.18	38.55	0.05			
Lyr XR-1 ^a	18	18	36	0.17	0.17	5.1	1.91
Ag1 XR-1 ^a	19	12	0.0	0.13	0.13	5.1	-0.34
Vul XR-1	20	38	29	0.15	0.15	5.5	-0.76
Cas XR-1	23	21	58.5	0.3	0.3	3.9	-0.14
Tau XR-1 ^b	5	31	22.1	2.7	2.7	1.3	-0.11
Cep XR-1	0	15	66	0.3	0.3	3.9	0.27
Lac XR-1 ^a	22	34	53.8	0.17	0.17	5.1	-0.44
Cep XR-2 ^a	22	42	62	0.18	0.18	5.0	0.18
Cep XR-3 ^a	23	54	72.9	0.15	0.15	5.5	1.04

a. Source observed only one scan; pitch uncertainty is $\pm 4 \text{ deg}$ [2].

b. Sources which definitely show power spectra. They are not included in calculating the number of X-ray sources as a function of gas mass.

TABLE 2. GALACTIC SUPERNOVAE [3]

Year	m_{\max}	α_{1900} (deg)	δ_{1900} (deg)	Remnant
185	?	215	-60	Rad ^a
396	-3m	60	+20	Rad
437	?	100	+20	---
827	-10	255	-30	Rad
1006		225	-50	Rad
1054	(-6)	85	+22	Rad, CM Tau ^b
1181	?	25	+70	---
1203	0	255	-40	---
1230	?	275	+20	---
1572	-4, 1	4.75	+64	Rad + B Cas ^c
1604	-2, 6	261.25	-21	Rad + V 843 Oph ^d

a. Rad: Radioquelle — radio source

b. Crab Nebula

c. Tycho's Nova

d. Kepler's Nova

The diameter of the X-ray source, as deduced by Friedman et al. [2] during a lunar occultation, is about $1.9 \cdot 10^{16}$ m, as compared to a diameter of about $5.676 \cdot 10^{16}$ m in visible radiation and to a diameter of about 20 km if the source were the hot surface of a cooling neutron star. In addition to the extent of the source, the shape of the spectrum shows that the observed X-radiation comes primarily from the filamentary part of the Crab Nebula rather than from a residual hot neutron star.

The ultrarelativistic electrons emitting most of the power radiated in synchrotron radiation have lifetimes against synchrotron losses shorter than the age of the nebula. These electrons have to be resupplied continually with an energy rate of 10^{31} W to counterbalance the synchrotron losses. Compressional waves are observed to damp out with a power loss of the same order

of magnitude as the power radiated in synchrotron radiation. It is supposed that the damping of the compressional waves acts as the energy source for the acceleration. Variations in the surface brightness, which are usually referred to as "wisps," moving in a time scale of months are observed near the center of the nebula. The dimensions of a wisp may be as great as $1.892 \cdot 10^{15}$ m, and its energy content is about 10^{37} to 10^{38} J. These variations in optical synchrotron radiation are interpreted as local compressions in the magnetic field. The observed damping of the motions implies a loss of energy at a rate of about 10^{31} W. The dynamo effect and the emission and reabsorption of fluid dynamic waves are the bases for the acceleration, which is confined to the central region. This damping supplies sufficient power to balance the synchrotron losses. In the central region, the power input to the electrons has to be balanced by losses caused by the escape of electrons to the outer region where most of the power in synchrotron radiation is radiated.

The energy source exciting the fluid-magnetic waves and supplying 10^{31} W is centrally located and may be a thermal source in the far ultraviolet, although none has been observed.

Spectral data from the Crab Nebula are fitted by the following expression:

$$\frac{dN}{d\epsilon} = 1.63 \cdot 10^{-11} \text{ photons m}^{-2} \text{ sec}^{-1} \text{ J}^{-1}$$

$$3.2 \cdot 10^{-16} < \epsilon < 1.76 \cdot 10^{-15} \text{ J} \quad .$$

For the total emission, the following values have been obtained:

$$TE = 2.4 \times 10^{-11} \text{ W m}^{-2} (3.2 \cdot 10^{-16} < \epsilon < 1.76 \cdot 10^{-15} \text{ J}) \quad ,$$

$$TE = 1.9 \times 10^{-11} \text{ W m}^{-2} (3.2 \cdot 10^{-16} < \epsilon < 8.0 \cdot 10^{-16} \text{ J}) \quad ,$$

$$TE = 1.6 \times 10^{-11} \text{ W m}^{-2} (3.2 \cdot 10^{-16} < \epsilon < 8.0 \cdot 10^{-16} \text{ J}) \quad .$$

It is possible to approximate the spectrum with two power laws. Between $4.81 \cdot 10^{-15}$ and $8.01 \cdot 10^{-15}$ J, a $W^{-4.4}$ spectrum is obtained; between $8.01 \cdot 10^{-15}$ and $1.19 \cdot 10^{-4}$ J, a $W^{-9.2}$ variation may be fitted to the data.

An X-ray pulsar in the Crab Nebula is identical to the radio and optical pulsar NP 0532. The X-ray pulsed flux amounts to about 5 percent of the integrated X-ray flux of the entire nebula (3 to $15 \cdot 10^{-10}$ m). If the total X-ray

flux (1 to $10 \cdot 10^{-10}$ m) is about $3 \times 10^{-11} \text{ W m}^{-2}$, then the corresponding X-ray pulsar flux is $1.5 \times 10^{-12} \text{ W m}^{-2}$. The pulsar X-ray power is about 200 times the optical power and 2×10^4 times the radio power. The X-ray and γ -ray pulsed intensity is 7 percent of the Crab Nebula. This is equivalent to an average pulsed power of $1.6 \times 10^{-12} \text{ W m}^{-2}$ at the top of the earth's atmosphere. The percentage of pulsed luminosity is of the same order as that observed in the soft X-ray region, indicating a softening of the pulsed spectrum between the optical and the hard X-ray regions.

The principal properties of pulsars can be explained if a falling core rebounds at finite or infinite density, as assumed in the oscillating model of the universe. A possibility is that the bounce occurs in the neighborhood of the Planck density:

$$\rho_e^* = \frac{c^5}{G^2 \hbar} \approx 10^{97} \text{ kg m}^{-3} .$$

The intermediate configurations then become pulsating structures, and the rise and fall of the core is the basic regulating principle. During the collapsing phase, radiation from the envelope is comparatively weak; in the rising phase the core and its adjacent shells emit a blast of intense blueshifted radiation. Catastrophic collapse results in a bouncing core structure, the outer layers of which are supported by the periodic radiation blasts from the core.

Cyg X-2. Cyg X-2 is a semidetached binary in which the X rays are generated by matter flowing from a G star through the L_1 point (the gravitational balance point in the rotating coordinate system of the binary) and being accreted on a compact object, which may be assumed to be a white dwarf. The requirement would be $10^{-8} M_{\odot}$ per year. Expected trajectories for such material have been computed by Kopal [4]. The gas will lose orbital energy when it enters the region of relatively high density which should exist near the white dwarf. The gas will therefore lose energy and fall on the white dwarf. Orbital motion provides a periodic component to the observed fluxes when one part of the system occults another. Fluctuations in the transfer of matter from one star to the other can lead to irregular variations. Peaked oscillations of amplitude of about 0.04 magnitude with rise and fall times of the order of 3 min, with intervals of approximately 11 min, are visible by inspection in optical flux of the candidate star. These are superimposed on a longer-term fluctuation of about a 1-hr period, of amplitude 0.10 magnitude, superimposed in turn on a gradual decline of about 15 percent over a 5-hr interval. A computed Fourier power spectrum confirms these visual impressions and shows other components. The spectrum is definitely nonwhite.

There is some indication from the photometric data that the system may be an eclipser. The rotational motion of the object with respect to the galaxy must be quite small and the eccentricity of its galactic orbit quite large. On this evidence, Cyg X-2 must be classified as a Population II object.

The spectrum of the candidate object for Cyg X-2 contains numerous sharp metallic lines identifiable with a star of spectral type G, probably a subdwarf. It is not certain if the short-term variations in brightness are those of the subdwarf or of some other source of energy. HeII in emission and CaI in absorption vary together in radial velocity. A short-period oscillation of 5.7 hr is suggested by the data, but longer time-scale variations of the mean velocity of the oscillation suggest the presence of a third body in the system, although other interpretations are possible. The general behavior of CaII and H γ suggests the presence of gaseous streams. The distance to the X-ray source is $1.54 \cdot 10^{16}$ to $2.16 \cdot 10^{16}$ km.

In close binaries, gas streams originate when the primary overflows its lobe of the critical Lagrangian surface. The mass transfer will take place to the secondary. The energy is released largely in the form of deceleration radiation X rays in the $1.6 \cdot 10^{-16}$ J range. The total luminosity in the X-ray flux is about 10^{28} W. The only other mechanism of energy dissipation is radiation of gravitational waves. The gravitational radiation amounts to about 10^{25} W if both components have masses of $1 M_{\odot}$. Variability in the X-radiation can be caused by changes in the rate of, or to the cessation of, mass transfer. The spectrum shows that the object is somewhat colder than Sco X-1 but that it possesses the same spectral characteristics.

Sco X-1. Sco X-1 is starlike, smaller than 0.5 arcsec, or $1.496 \cdot 10^{13}$ m, and is barely detectable at radio wavelengths. More than 99 percent of its total luminosity is concentrated in the X-ray range.

The X-radiation is produced by free-free transitions in pure hydrogen. In the near-infrared spectral region, the gas is opaque and radiates as a black-body with a temperature of approximately 5×10^7 °K. All the radiation is produced by the same mass of gas which may be assumed to be spherical with a radius of $0.01 R_{\odot}$ and a density $\approx 10^{22}$ electrons m^{-3} . It requires a star with mass $\approx 0.1 M_{\odot}$ if the energy is supplied by gravitational infall of material.

The best fit of the observed counts to the deceleration spectrum yields a temperature of 4.8×10^7 °K. A large part of the optical radiation cannot be the optical extrapolation of deceleration radiation emitted by an optically thin layer of a hot plasma. This is indicated by the pulsational character of the light variation and the well-defined color variations. The majority of the observations of all nights during a total time of 24 hr distributed over 1966,

1967, and 1968 forms a mean light curve with a period of 0.^d5276, with an amplitude of 0.75 magnitude in blue light, and with an asymmetry (fraction of the light curve occupied by the descending branch) of 0.7.

The distance to Sco X-1, based on the X-ray absorption, is $8.33 \cdot 10^{18}$ m. This is to be considered as the minimum distance.

The energy source is assumed to be a close binary whose streaming plasma transfers are accompanied by shock collisions, therefore draining energy essentially from the gravitational and thermal store of the stars. The optical emission comes from a cooler plasma volume, only partly ionized.

The intensity at $9.61 \cdot 10^{-16}$ J is absolute intensity ($9.61 \cdot 10^{-16}$ J) = $5.22 \cdot 10^{-12}$ photons $\text{m}^{-2} \text{sec}^{-1} \text{J}^{-1}$.

The observed flux equals $L(1.6 \cdot 10^{-16} - 1.6 \cdot 10^{-14} \text{ J}) \approx 5 \times 10^{29} \text{ W}$, if the distance is about $8.33 \cdot 10^{18}$ m.

$$\text{TE} = 1.1 \times 10^{-10} \text{ W m}^{-2} (3.2 \cdot 10^{-16} < \epsilon < 8.0 \cdot 10^{-16} \text{ J}) .$$

The observed spectrum yields a spectral flux of photons characteristic of deceleration radiation from a hot thin gas, thus

$$\frac{1}{\epsilon} e^{-\frac{\epsilon}{kT}} .$$

The data can then be fitted with

$$kT = 6.41 \cdot 10^{-16} \text{ J} .$$

The measured intensities of Sco X-1 are reproduced as given in Table 3.

The recoil photon, which is registered, was scattered when the energy density of blackbody radiation was much greater than at present. However, to explain the diffuse X-ray background, there must have existed more or stronger sources of electrons in the past than at present. It is probable that the intergalactic gas density was greater in the past and has decreased as galaxies have evolved and stars formed. Such an effect would tend to increase the calculated X-ray background.

TABLE 3. INTENSITIES OF SCO X-1 X RAYS [5]

Date	Intensity ($1.602 \cdot 10^{-12}$ photons $m^{-2} sec^{-1} J^{-1}$)	Field of View (half angles, deg)	Accuracy of Attitude	Calibration
Oct 1, 1964	4.0	1.5×18.3	Reasonable	Pre- and post-flight
Jun 12, 1965	5.5 ± 0.4	10×45	Poor	Nose cone
Jul 26, 1965	5 ± 1	~ 20 elliptic	Poor	Preflight
Oct 28, 1965	3.8 ± 0.3	7×30	Reasonable	Nose cone
Mar 8, 1966	3.7 ± 0.4	1×40	Good	Preflight
Jul 28, 1966	3.7 ± 0.4	2.5×8	Good	Nose cone
Oct 11, 1966	3 ± 0.6	1×40	Good	Preflight
Feb 6, 1967	3.3 ± 0.9	10×30	Good	Inflight
May 18, 1967	2.8 ± 0.3	10×30	Good	Nose cone
Sep 29, 1967	3.3 ± 0.7	10×30	Good	Nose cone
Oct 2, 1967	3.8 ± 1	5×30	Good	Nose cone

A best fit to all the present diffuse X-ray data gives the following results:

$$\frac{dN}{d\epsilon} = 1.99 \cdot 10^{-11} \text{ photons } m^{-2} \text{ sec}^{-1} \text{ J}^{-1} \text{ sr}^{-1} .$$

The intensity of the diffuse component of cosmic X rays has been found to be essentially constant. The intensity at $9.61 \cdot 10^{-16}$ J is:

$$\frac{dN}{d\epsilon} (9.61 \cdot 10^{-16} \text{ J}) = 9.6 \cdot 10^{-13} \text{ photon } m^{-2} \text{ sec}^{-1} \text{ J}^{-1} \text{ sr}^{-1} .$$

The energy spectrum is nearly flat between $6.41 \cdot 10^{-16}$ and $1.44 \cdot 10^{-15}$ J;

$$\text{Absolute intensity } (5.77 \cdot 10^{-16} - 1.44 \cdot 10^{-15} \text{ J}) = 3.58 \cdot 10^4 \text{ photons } m^{-2} \text{ sec}^{-1} \text{ sr}^{-1}$$

Total emission: $7.6 \cdot 10^{-11} \text{ J m}^{-2} \text{ sec}^{-1} \text{ sr}^{-1}$ for $1.6 \cdot 10^{-16} < \epsilon$
< $2.08 \cdot 10^{-15} \text{ J}$

Total emission: $2.1 \cdot 10^{-11} \text{ J m}^{-2} \text{ sec}^{-1} \text{ sr}^{-1}$ for $3.2 \cdot 10^{-16} < \epsilon$
< $8.0 \cdot 10^{-16} \text{ J}$.

There is no large change in the spectral index between $1.6 \cdot 10^{-16}$ and $9.61 \cdot 10^{-15} \text{ J}$. Above $1.6 \cdot 10^{-14} \text{ J}$, the spectrum steepens to a value of about 2. For $1.6 \cdot 10^{-11} \text{ J} < \epsilon$ there are indications of additional steepening.

Therefore, the presently available experimental results for the diffuse X-ray flux from $1.6 \cdot 10^{-16}$ to above $1.6 \cdot 10^{-11} \text{ J}$ cannot be represented by a simple power law. The spectral index has a value of about 1.7 from $1.6 \cdot 10^{-16}$ to $9.61 \cdot 10^{-15} \text{ J}$, then increases to about 2. These values are in agreement with the prediction of Felten and Morrison [6] based upon the inverse Compton effect. Their calculated values for the spectral index are 1.7 between $1.6 \cdot 10^{-16}$ and $1.6 \cdot 10^{-14} \text{ J}$, and a larger value at higher energies.

No dependence of the flux on galactic latitude was found within a limit of about 8 percent in sampling intervals of 30 deg. This result is in agreement with an extragalactic origin for the X-ray background.

It is possible to explain the background of soft X-ray emission ($\lambda \approx 2 \cdot 10^{-9} \text{ m}$) by the integral emission of all the galaxies in the metagalaxy. The intensity measurements on Sco X-1 are consistent with the assumption that between $3.2 \cdot 10^{-16}$ to $3.2 \cdot 10^{-15} \text{ J}$ more X-ray intensity is radiated when close to maximum intensity than when at minimum or average intensity. The change in X-ray intensity is not as great as the change in optical intensity.

Cen X-2. Cen X-2 is within the error radius of a variable star which exhibits night-to-night variations with a total observed range of 0.4 magnitude. The star has not undergone violent outbursts during a 60-yr optical observation. The distance is estimated at $1.542 \cdot 10^{19} \text{ m}$, which is comparable with Sco X-1.

Cen X-2 is a highly variable X-ray star. The variability of the X-ray flux is shown in Table 4. The decrease in X-ray flux during the period April through May 1967 can be represented as an exponential decay with a time constant of 23.4 days. This decrease was also accompanied by a softening of the spectrum. The Cen X-2 source gives recurring X-ray outbursts, each outburst lasting only for a short period of time.

TABLE 4. TIME VARIATION OF X-RAY INTENSITY
FROM CEN X-2 [7]

Experimenter	Flight Date	Energy in 3.20-8.01 · 10 ⁻¹⁶ J Range (10 ⁻¹¹ J m ⁻² sec ⁻¹)
Grader et al. [8]	Oct 28, 1965	<0.25
Harries [7]	Apr 4, 1967	11.0 ± 1.0
Cooke et al. [9]	Apr 10, 1967	16.0 ± 1.0
Francey	Apr 20, 1967	7.5 ± 1.0
Chodil et al. [10]	May 18, 1967	2.6 ± 0.4
Chodil et al. [11]	Sep 28, 1967	<0.3
Lewin, Clark, and Smith [12]	Oct 15, 1967	0.62 (Extrapolated)
Pounds	Jun 12, 1968	<0.1
Rao et al. (Present Experiment)	Nov 3, 1968	0.68 ± 0.08
Rao et al. (Present Experiment)	Nov 7, 1968	0.83 ± 0.14

Cas A. In the study of the motions of the luminous filaments associated with the radio source Cas A, the following center of expansion is found:

Period	α (1950)	δ (1950)
1951-1968	23.38 deg	58.58 deg

Assuming a uniform rate of expansion, the explosion which generated Cas A is found to have occurred in 1667 AD ± 8. Adopting a value $22.5 \leq V$ for the stellar remnant of Cas A, this value is 6 magnitudes fainter than the value $V = 16.5$ which has been obtained for the pulsar in the Crab Nebula. The distance of the Crab Nebula is $6.17 \cdot 10^{19}$ m, which may be compared with a distance of $1.05 \cdot 10^{20}$ m for Cas A. Then the remnant of Cas A must be at least 5 magnitudes (100 times) fainter than the central star of the Crab Nebula.

It may be assumed that the absorption in the direction of Cas A is very much greater than in the direction of the Crab Nebula. The fact that the super-nova outburst of 1667 AD was not observed supports the assumption that the absorption in the direction of Cas A is large.

Diffuse Background Radiation. The diffuse X-ray background has been established as independent of galactic coordinates to within 10 percent. The power law shape of the received spectrum has the form:

$$I_{\nu} \approx \nu^{\frac{1-m}{2}},$$

$$m = 3.4$$

between $8.0 \cdot 10^{-16}$ and $1.6 \cdot 10^{-13}$ J. The spectral shape results from the Compton effect where recoil photons are generated by collisions between the universal 3°K distribution and a leakage spectrum of cosmic-ray electrons from radio galaxies. However, the added flux from all galaxies within a Hubble distance falls short of the observations by a factor of about 10^2 in intensity.

The energy spectrum of the diffuse cosmic X-ray background between $3.2 \cdot 10^{-15}$ and $3.52 \cdot 10^{-14}$ J fits closely a single power law:

$$I(W)dW = 3.124 \cdot E^{-2.45} dW \text{ photons sec}^{-1} \text{ m}^{-2} \text{ sr}^{-1} \text{ J}^{-1} .$$

Unidentified X-Ray Sources

Since only a few of the known X-ray sources coincide with identifiable optical objects, a statistical study has been undertaken to collectively investigate the population characteristics of the galactic X-ray sources. The degree of correlation existing between the positions of X-ray sources and classical cepheids, galactic novae, planetary nebulae, and Wolf-Rayet stars has been determined. Since all these objects have low galactic latitudes, only the correlation in galactic longitude was examined; then each object forms a point on the galactic circle. The circle was partitioned into a number of equal intervals, and the correlation coefficient was calculated by comparing the number of X-ray sources per interval to the number of the compared type per interval.

The results are contained in Table 5. It is seen that the correlation coefficient is large for the planetary nebulae and novae in comparison with cepheids and Wolf-Rayet stars. Assuming that, despite the uncertainty regarding the completeness of the surveys used, the data in Table 5 are representative for the actual distributions in the galactic plane of the various types of objects, the small correlation coefficients for the cepheids and Wolf-Rayet

TABLE 5. CORRELATION COEFFICIENTS [13]

Type of Object	Interval Size						
	4 deg	6 deg	8 deg	9 deg	10 deg	12 deg	15 deg
Cepheids (361)	0.05	0.07	-0.01	0.04	0.01	-0.03	0.02
Novae (92)	0.49	0.52	0.63	0.56	0.55	0.60	0.60
Planetaries (1024)	0.56	0.61	0.69	0.63	0.62	0.69	0.67
Wolf-Rayet (127)	0.08	0.10	0.15	0.14	0.32	0.17	0.26
NOTE: The number in parentheses represents the objects used in comparison.							

stars imply that X-ray sources are not associated with these extreme Population I objects. The good correlation between X-ray sources and the galactic novae and planetary nebulae implies that X-ray sources are more strongly associated with Population II than with extreme Population I objects.

Discussion of the Results

It has been shown that the X-ray sources in space that have been identified are either former supernovae emitting synchrotron radiation or close binary systems emitting deceleration radiation. The final state of a supernova is a superdense star. Since X-ray astronomy has advanced the knowledge of superdense stars and of close binary systems, the properties of these objects will be discussed.

Superdense Stars. A star of 2 to 10 solar masses and density 10^{10} to 10^{11} kg m^{-3} gradually loses energy and contracts. It becomes unstable against collapse and finally undergoes a supernova explosion. Under appropriate conditions, the explosion leaves behind a superdense core. This star rotates, vibrates, and radiates. The radiations include neutrinos, X rays, long-wavelength electromagnetic waves, and gravitational waves. So far, no superdense star has been identified. The properties of superdense stars have been evaluated under the following assumptions:

1. Temperature less than 10^8 °K.
2. The matter catalyzed to the end point of thermonuclear evolution.

3. Magnetic induction B less than:

$$\frac{m^2 c^2}{e \hbar} = 4 \times 10^9 \text{ tesla} = 4 \times 10^{13} \text{ gauss} .$$

4. Tangential velocity of surface less than $\frac{c}{15}$.

No continuous transition occurs from stable cold dwarf stars to stable cold superdense stars. The equilibrium is unstable for the range of intermediate configurations. A dwarf star can jump across this gap and be transformed into a superdense star only by a nonequilibrium process like the explosion of the outer part of a supernova and the implosion of its interior.

The instability in the gap between stable dwarfs and stable superdense stars has its origin in the process:



In consequence of this process, pressure increases less rapidly with compaction in stage of electron crush than it does at lower and higher pressures. For nonrelativistic gases over a limited range of variation, the variation of pressure with density can be characterized by a law of the form:

$$p = C \times s^{\gamma_0}$$

$$\gamma_0 = \frac{s}{p} \frac{dp}{ds} .$$

A modified relation applies to relativistic gases:

$$\gamma_0 = \frac{p^* + s^*}{p^*} \frac{dp^*}{ds^*} ,$$

which reduces to the nonrelativistic result in the limit. The terms p^* and s^* are geometrical units used in general relativity. The conversion is shown in Table 6.

In the Newtonian approximation, the equilibrium is stable only if $3\gamma_0$ exceeds 4, or when the average γ_0 exceeds $4/3$. The gap of instability extends over a range of central densities from 3×10^{11} to $3 \times 10^{16} \text{ kg m}^{-3}$. The transition from the Newtonian theory to general relativity produces only a slight change in the analysis.

TABLE 6. CONVERSION FROM CONVENTIONAL UNITS
TO GEOMETRICAL UNITS [14]

	Conventional	Geometrical
Mass of sun	$M_{\odot} = 1.987 \times 10^{30} \text{ kg}$	$M_{\odot}^* = 1.474 \text{ km}$
Standard baryon (1/56 of Fe^{56})	$\mu_s = 1.659 \times 10^{-27} \text{ kg}$	$\mu_s^* = 1.231 \times 10^{-57} \text{ km}$
Typical density	$\rho_e = 2 \cdot 10^{17} \text{ kg/m}^3$	$\rho_e^* = 1.48 \times 10^{-14} \text{ cm}^{-2}$
Energy	$E (10^{-7} \text{ J})$	$M^*(\text{cm}) = 0.8258 \times 10^{-49} E$
Time	$t_{\text{conv}} (\text{sec})$	$t(\text{cm}) = ct_{\text{conv}} = 2.997925 \times 10^{10} t_{\text{conv}}$
Pressure	$p \cdot 10^{-1} \text{ newton/m}^2$	$p^*(\text{cm}^{-2}) = (G/c^4)p$

A sphere of matter of uniform density and adjustable radius r will be considered. A baryon number

$$A = 0.74 \times 10^{57} ,$$

about three-fourths of the baryon content of the sun, is selected. For very large r , the calculated mass-energy is the mass of the corresponding number of Fe^{56} atoms, dispersed at infinite dilution, without gravitational binding. As r decreases, the gravitational energy and elastic forces increase in significance. When the density reaches 10^9 kg m^{-3} , the rate of rise of the contribution of the elastic forces to the energy balances the rate of fall of the increasingly negative gravitational energy. Here, the total reaches a minimum value of $-5 \times 10^{42} \text{ J}$, which is characteristic for the white dwarf configuration. With further compaction, the energy required for compression increases faster than the energy set free by gravitational attraction. At a density of $5 \times 10^9 \text{ kg m}^{-3}$, the net energy of interaction changes from negative to positive, and at a density of $10^{14} \text{ kg m}^{-3}$, the net energy reaches a maximum value of $2 \times 10^{44} \text{ J}$, which forms an energy barrier. The phenomenon of the electron crush has its beginning. Consequently, the pressure provided by the matter does not rise as rapidly as the pull of gravity. At a density of $2 \times 10^{15} \text{ kg m}^{-3}$, the interaction energy turns back from positive-characteristic for compression to negative-characteristic for gravity. As the density increases, it becomes more negative. As the crushing of electrons onto protons to produce neutrons is almost complete, the density approaches nuclear values. Compressive forces regain the ability to compensate gravitational forces and balance occurs. At a density of $10^{17} \text{ kg m}^{-3}$, the

interaction energy reaches a minimum of 10^{-45} J, characteristic for the neutron star configuration at the second stable equilibrium. As the density is raised above 10^{17} kg m⁻³, work done against the nuclear forces rises faster than the energy supplied by gravitational forces. At a density of about 10^{18} kg m⁻³, the net binding becomes zero. With further increase in density, the net energy becomes increasingly positive, similar to the energy of a spring, tightly compressed and ready to expand explosively if released.

To summarize the result, a system of

$$A = 0.74 \times 10^{57} \text{ baryons}$$

constrained to a spherically symmetric and homogeneous configuration possesses four states of equilibrium. Two of these are stable (the uniform models for white dwarf and neutron stars) and two are unstable. One of the unstable configurations lies at the summit of a potential energy hill, separating the white dwarf from the neutron star configuration. The other configuration lies at the summit of a much higher potential hill, which separates existence as a neutron star from a state of complete collapse. At a certain critical baryon number, which is uncertain, the barrier between the neutron star configuration and the collapsed state disappears. For values of A of this magnitude and more, a stable neutron star configuration exists no longer. At another critical baryon number, about 1.18 times the baryon content of the sun, the barrier between white dwarf and much denser configurations disappears, and no stable white dwarf configuration exists.

There is no indication of the existence of a third family of stable forms of equilibrium in a configuration of still higher density.

By some process of accretion, the mass of a neutron star may be raised above the critical limit. Achievement of supercriticality is followed by collapse of the neutron star which proceeds slowly at first then more rapidly. In gravitational collapse, the matter arrives in a finite proper time at a state of unlimited density. Where the matter is located and in the empty space around the matter for some distance, the curvature of space tends to infinity. A distant observer will not obtain light signals from these regions, but he will obtain a last ray from the surface of the infalling matter in an infinite proper time of his location. The surface material continues to emit radiation after the last ray, but these photons are caught in the constricting curvature of the immediately surrounding empty space. The conditions ultimately encountered by the collapsing matter and by the geometry of collapse for some distance outside the matter become so singular that the classical version of the general

theory of relativity has to be replaced by the quantum version of that theory, in which quantum-mechanical probability amplitudes exist for several final states. The range of the final states for which the probability amplitudes take on significant values is not known. On the time scale of the distant observer, the collapse does not terminate. A system in continued gravitational collapse shows ever-decreasing luminosity but continues to exert full gravitational attraction forever.

A list of the galactic supernovae is contained in Table 2.

A comparison is made between the characteristics of types I and II supernovae in Table 7. Diagrammatic representations of the light curves of these types are shown in Figures 1 and 2.

TABLE 7. TYPES OF SUPERNOVAE [14]

Type of Supernova	Type I	Type II
Ejected hydrogen?	No	Yes
Predominant association with what stellar population?	Old stars (Galactic halo)	Young stars (Galactic disk)
Presumptive mass of precursor	1.16 to $2M_{\odot}$	$>2M_{\odot}$
Total optical energy	$4 \cdot 10^{42}$ J	$2 \cdot 10^{42}$ J
Peak luminosity	10^{36} W	10^{36} W
Typical ejected mass	0.1 to $1M_{\odot}$	1 to $10 M_{\odot}$
Concomitant observed kinetic energy	$4 \cdot 10^{41}$ to 42 J	$4 \cdot 10^{43}$ to 44 J
Relative frequency of the two types	less	more

The Crab Nebula is the remnant of the 1054 type I supernova. The pulsar NP 0532 with a period of 0.033 sec is close to its center. The period of the Crab pulsar is lengthening by 3.70×10^{-8} sec per day. Extrapolating the period back to 1054 gives 20 msec. A second pulsar has been found only 1.2 deg from the Crab Nebula. If the two pulsars were formed in the same supernova explosion, the velocity of the second must be at least 15 percent that of light. On the assumption that NP 0532 is a neutron star rotating as a rigid body, the period change implies an energy loss of 10^{31} W. During this period, the nebula loses about 10^{31} W by expansion and from radiation by its relativistic electrons. The equivalence of these numbers suggests that the energy for the nebula's expansion and for the high-speed electrons comes from the neutron star's rotation, but it is not obvious how the rotational energy can be converted into particle energies.

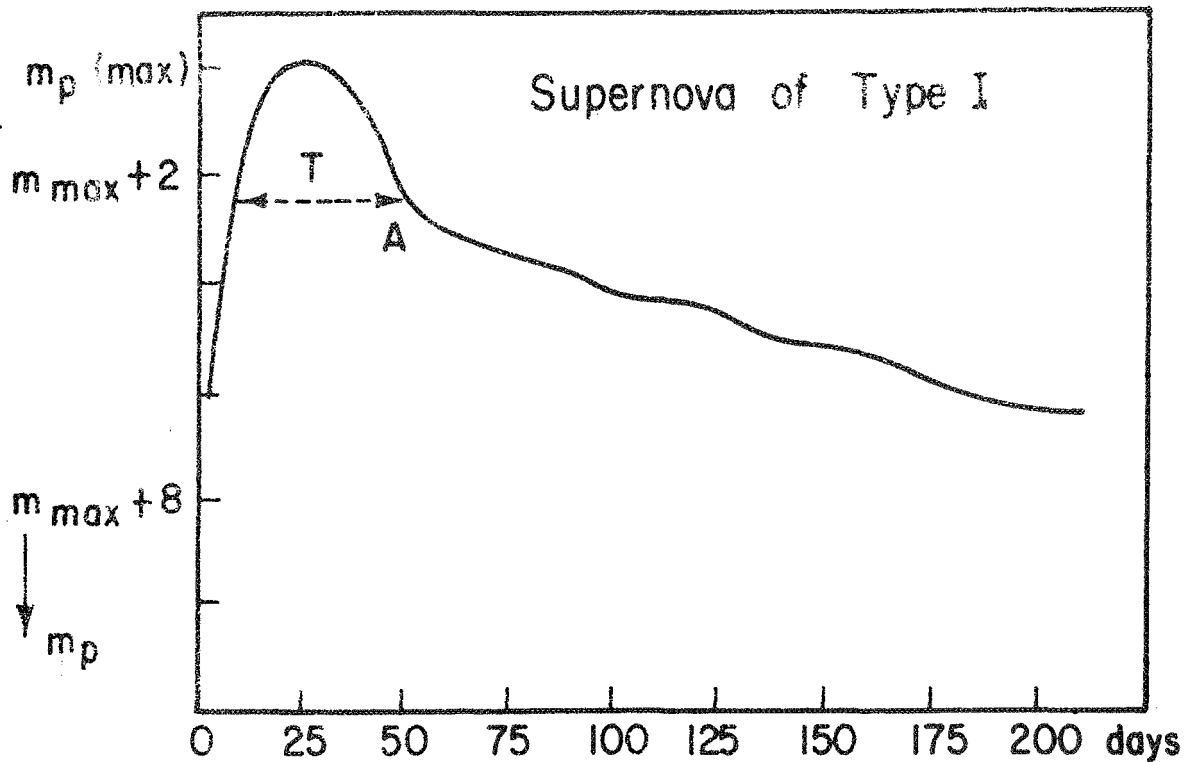


Figure 1. Schematic representation of light curve of type I supernova [15].

The X-ray flux of the pulsar NP 0532 has been found to vary by 6.5 ± 2.7 percent in a period of 0.033 sec. The energy distribution of NP 0532 fits that of a blackbody at 10 000°K after a correction for interstellar reddening.

Close Binary Systems. The hypothesis is made that a binary system originates from the splitting of a single star into two components because of rotational instability during the contraction of the star. At the present state of the theory it is difficult to give a reliable criterion for fission rather than equatorial mass loss. It is known that a rotating fluid reaches a point of bifurcation when

$$\alpha = \frac{\omega^2}{2\pi G s} = 0.187 \quad .$$

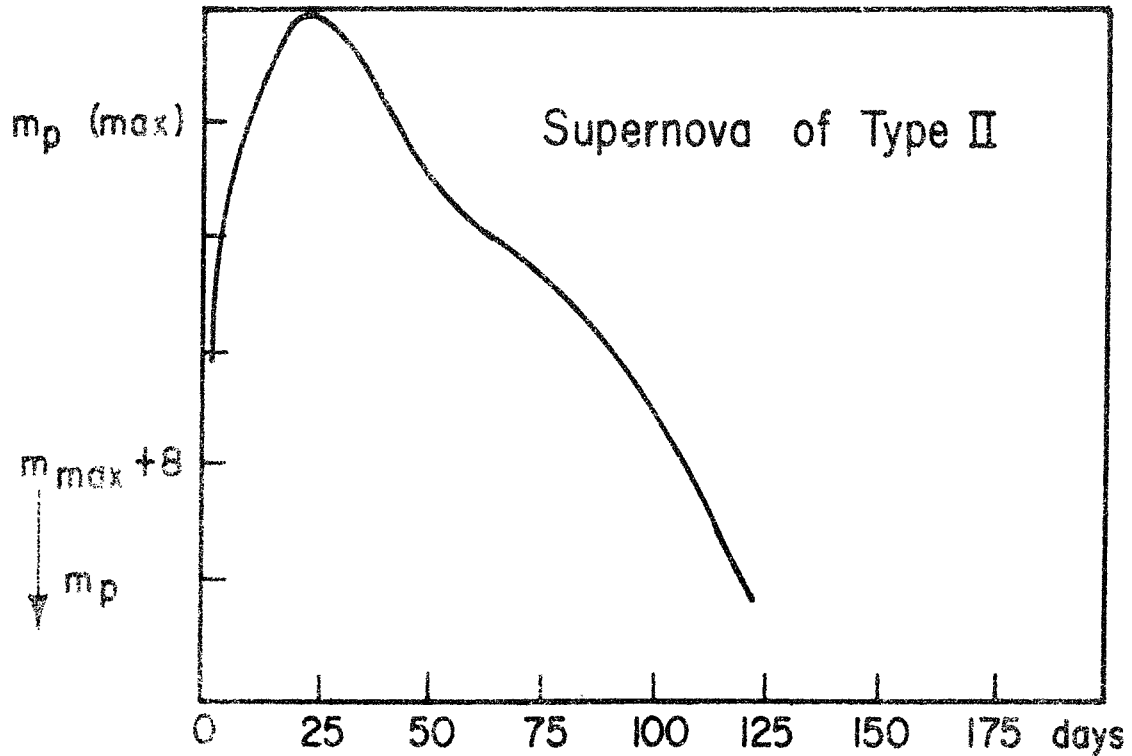


Figure 2. Schematic light curve of supernova of type II [15].

It will be assumed that a star becomes rotationally unstable and splits into two parts when

$$\alpha = \frac{\omega^2}{2\pi G s_c} = 0.187 \quad ,$$

where s_c denotes the density at the center.

The dynamical collapse of a gas cloud and the subsequent evolution of a spherical star until it becomes a main sequence star occurs along a Hayashi track. If the star rotates, its evolutionary pattern will differ from that of a spherical star. Once the star becomes dynamically stable, the subsequent contraction can be investigated assuming uniform rotation. The star contracts losing matter from the equator, thereby changing its angular momentum, and contracts down almost vertically in the H-R diagram, losing mass and angular momentum. During this period, it is fully convective until it reaches a point where the energy can be transported by radiation and a radiative core begins

to develop. As long as the star was completely convective, the turbulence distributed the angular momentum throughout the star so that uniform rotation was a valid approximation. With the growth of the radiative core, the inner regions — disregarding possible magnetic fields — are no longer coupled to the outer regions, and the star does not rotate uniformly even approximately any longer. Each element of the radiative core contracts, therefore conserving its angular momentum as the star continues to lose mass from the convective envelope. With the uncoupling of the central region from the surface by the development of the radiative core, the rotational effect becomes significant in the central region. The parameter can then be calculated at any stage during the contraction, and if it becomes larger than the limit of stability 0.187, the central region will become unstable and split into two parts.

According to this theory, single and double stars are formed by similar processes. Then, the chemical composition in each pair was the same initially, but their masses may have been different. The difference in mass was responsible for the difference in the subsequent evolution. If the masses were unequal at the time of the formation of the system, the more massive component will develop an incipient hydrogen shortage and subsequent expansion ahead of its less massive and luminous companion.

The Roche model of a close binary system consists of two components with a mass concentration so high that their gravitational potential can be approximated by that of a mass point. In a rotating Cartesian coordinate system with the origin at the center of gravity of component m_1 , with the x-axis joining the two components, and with the y-axis lying in the orbital plane, the surfaces of constant potential are described by the formula:

$$c = \frac{2}{1+q} \frac{1}{r_1} + \frac{2q}{1+q} \left(\frac{1}{r_2} - x \right) + x^2 + y^2 + \frac{q^2}{(1+q)^2} ,$$

$$q = \frac{m_2}{m_1} ,$$

where r_1 and r_2 denote the distances measured from the centers of gravity of the respective components. The distance between the components is taken as unit of length. A section of the equipotential surfaces by the orbital plane is shown in Figure 3, which has been drawn to scale for $g = 0.215$. The two separate lobes coalesce in the surface containing the first Lagrangian point L_1 . The two lobes of this particular surface represent the upper limits to the size of the components, if they are to be considered as separate stars. This surface is called the Roche limit; the two lobes are called the Roche critical lobes.

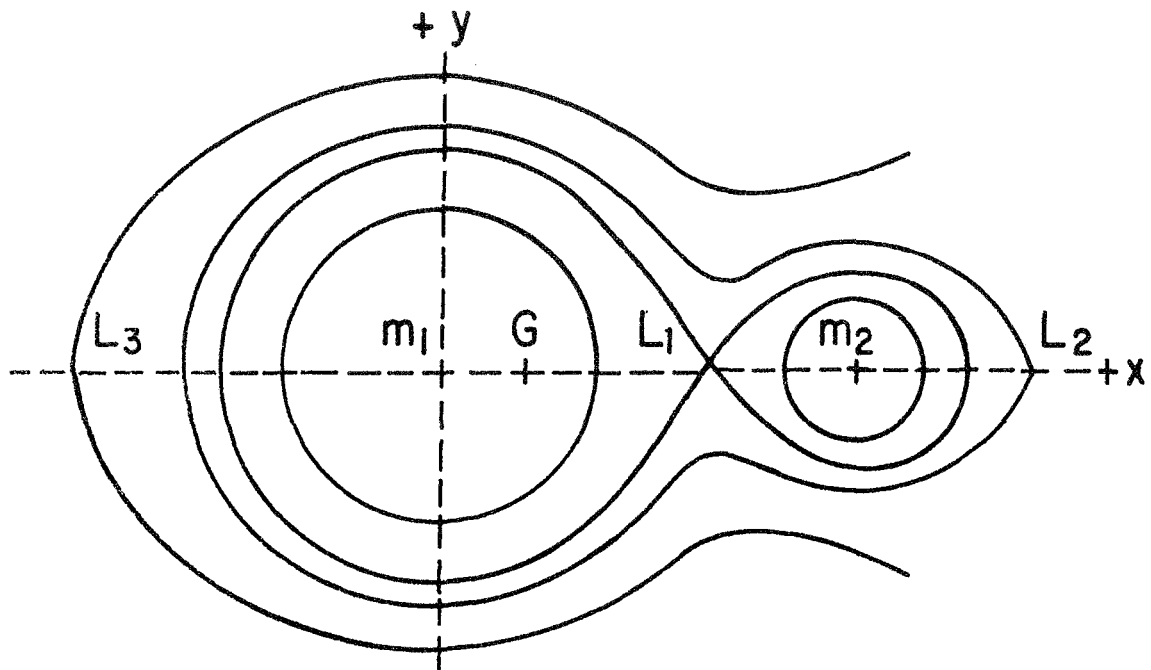


Figure 3. Equipotential curves of the Roche model in the orbital plane (Roche limit marked by heavy line) [16].

Close binaries are those systems in which a component fills its critical Roche lobe at a stage of its evolution. Even in a close binary, the components evolve independently of each other as long as both remain smaller than the Roche limit.

A star can reach the Roche limit at phases when its outer layers expand. Essentially, two phases of expansion of the envelope exist: Phase A — slow expansion during hydrogen burning in the core and Phase B — rapid expansion when hydrogen is burning in the shell.

The stages of normal stellar evolution are as follows:

1. Pre-main sequence contraction.
2. Initial main sequence.
3. Main sequence.

4. Advanced main sequence.
5. Rapid expansion.
6. Core helium burning.

In systems which undergo mass exchange, not all stages of normal evolution occur. If mass exchange occurs at Phase A, stage 4 is terminated abruptly, and stages 5 and 6 do not exist.

In case of a mass exchange at Phase B, stage 5 is shorter, and stage 6 does not occur. It is replaced by the following stages:

1. Rapid mass transfer.
2. Slow mass transfer.
3. Contraction after mass transfer.
4. The final stage of evolution of the original primary.

The stages of large-scale mass loss are relatively short. In Phase A, in the system $7M_{\odot} + 5M_{\odot}$, the maximum rate of mass transfer is $4 \times 5^{-5} M_{\odot} \text{y}^{-1}$; in the system $5M_{\odot} + 3M_{\odot}$, the maximum rate is $2 \times 10^{-5} M_{\odot} \text{y}^{-1}$. It can be expected that for Phase B, and for more massive stars, the rates are an order of magnitude higher.

THE BACKGROUND X-RAY FLUX IN THE GALAXY

Introduction

The hypothesis is made that the background X-ray flux in the galaxy consists partly of synchrotron X rays which are generated in a galactic dynamo. Synchrotron radiation from the galaxy has been observed at radio frequencies. The radio emission of the galaxy provides evidence that magnetic fields extend far beyond the boundaries of the galaxy proper into a corona which is called the halo. The halo contains at least 5 percent of the total mass of the galaxy.

From the rotation of the plane of polarization by the Faraday effect in radio sources, it follows that the magnetic fields in the galaxy have intensities of the order of

$$10^{-5\pm 1} \text{ gauss} = 10^{-9\pm 1} \text{ tesla} \quad .$$

In the galactic disk, the field strength exceeds 10^{-9} tesla; in the galactic halo, it is less than 10^{-9} tesla. In the spiral arms, a value $3 \cdot 10^{-9}$ tesla is assumed, and in the galactic halo, a value of $6 \cdot 10^{-10}$ tesla is assumed. In Table 8, order of magnitude estimates have been assembled by Woltjer [17, 18] for some physical quantities of the media occurring in the galaxy. A representative value, 10^{-9} tesla of the induction field throughout the galaxy is given; this value may be too high.

For a fully ionized gas, without a magnetic field, the coefficients of electrical conductivity, kinematic viscosity, and heat conductivity are given by the expressions:

$$\sigma = 6 \cdot 10^{-4} \text{ T}^{3/2} (\Omega \text{ m})^{-1} \quad ,$$

$$\nu = 4 \cdot 10^3 \text{ n}^{-1} \text{ T}^{5/2} \text{ m}^2 \text{ sec}^{-1} \quad ,$$

$$\kappa = 2 \cdot 10^{-7} \text{ T}^{5/2} \text{ W m}^{-2} \quad .$$

The Background X-Ray Flux

There exists a universal X-ray background with an energy flux of about $7.6 \cdot 10^{-11} \text{ W m}^{-2} \text{ sr}^{-1}$ [19].

The energy spectrum of the diffuse cosmic X-ray background has been represented by the following power laws:

$$J(\epsilon) = 3.124 \cdot 10^{-10} \cdot \epsilon^{-2.45} \text{ photons sec}^{-1} \text{ m}^{-2} \text{ sr}^{-1} \text{ J}^{-1}$$

$$3.2 \cdot 10^{-15} < \epsilon < 3.52 \cdot 10^{-14} \text{ J} \quad .$$

The flattening of the spectrum observed at lower energies occurs below $3.204 \cdot 10^{-15} \text{ J}$, with a change in spectral index of one power. A break in the background spectrum occurs between $1.602 \cdot 10^{-15}$ and $3.204 \cdot 10^{-15} \text{ J}$ [20].

TABLE 8. PHYSICAL PARAMETERS IN THE GAS^a

Medium	L	n	T	B	λ	r_L	t_{coll}	t_{cyc}	v_s	v_A	t_A	t_σ	t_κ	t_{rad}
H I	10^{19}	10	10^2	10^{-5}	10^{10}	10^6	10^5	10^2	10^5	10^6	10^{13}	$(10^{16})^b$	$(10^{18})^c$	10^{15}
H II	10^{19}	10	10^4	10^{-5}	10^{11}	10^7	10^5	10^2	10^6	10^6	10^{13}	10^{31}	10^{19}	10^{11}
Halo	10^{22}	10^{-3}	10^6	10^{-5}	10^{19}	10^8	10^{12}	10^2	10^7	10^8	10^{14}	10^{40}	10^{16}	10^{17}

a. Legend (All in cgs units)

L	length scale	t_{cyc}	proton cyclotron period
n	hydrogen density	v_s	sound velocity
T	temperature	v_A	Alfvén velocity
B	magnetic field strength	t_A	time needed for an Alfvén wave to traverse distance L
λ	mean free path for a thermal particle with unit charge	t_σ	time scales on which effects of finite electric conductivity, heat conduction, and radiative losses become important
r_L	proton Larmor radius	t_κ	
t_{coll}	time interval between collisions for protons	t_{rad}	

b. Ambipolar diffusion.

c. Neutral particle thermal conductivity.

$$J(\epsilon) = 1.65 \cdot 10^{-11} \cdot \epsilon^{-1.35} \text{ photons sec}^{-1} \text{ m}^{-2} \text{ sr}^{-1} \text{ J}^{-1}$$

$$3.2 \cdot 10^{-16} < \epsilon < 3.2 \cdot 10^{-15} \text{ J} \quad [21]$$

$$J(\epsilon) = 1.99 \cdot 10^{-11} \cdot \epsilon^{-1.7} \text{ photons sec}^{-1} \text{ m}^{-2} \text{ sr}^{-1} \text{ J}^{-1}$$

$$1.6 \cdot 10^{-16} < \epsilon < 2.08 \cdot 10^{-15} \text{ J} \quad [19] \quad .$$

The Dynamo Theory of Galactic Magnetic Fields

A synchrotron origin of the background X-ray flux has been postulated before. Clark [22] has estimated that synchrotron X rays may constitute a major part of cosmic X rays incident from high galactic latitudes. He has calculated the expected X-ray intensity as:

$$3 \cdot 10^{-32} \text{ to } 3 \cdot 10^{-31} \text{ J sec}^{-1} \text{ m}^{-2} \text{ sr}^{-1} \text{ Hz}^{-1} \quad .$$

His estimations of the intensities of stellar and Compton X rays at $3 \cdot 10^{-10}$ m from high galactic latitudes are small compared to the intensity of synchrotron X rays. He concludes that synchrotron X rays may be an important, perhaps the dominant, component at high galactic latitudes at wavelengths below $3 \cdot 10^{-10}$ m.

Ginzburg and Syrovatsky [23] have examined the conditions under which synchrotron generation may be responsible for the emission of radiation in the X-ray band. They discussed the case of X rays with frequencies of the order of $\nu = 10^{18}$ Hz ($\lambda = 3 \cdot 10^{-10}$ m, $\epsilon = h\nu = 6.4 \cdot 10^{-16}$ J).

This frequency is emitted only by electrons with energies $E \approx 3.2 \cdot 10^{-2}$ J. It is concluded that the electrons which generate this radiation may originate in the cosmic ray sources.

Verma [24] has considered the possibility that the observed diffuse X-ray intensity in the $1.6 \cdot 10^{-16}$ to $6.4 \cdot 10^{-14}$ J region could partly be explained as synchrotron emission of ultra-high-energy halo electrons. He estimates that the synchrotron radiation, emitted by ultra-high-energy electrons, in the range from $1.6 \cdot 10^{-3}$ to $1.6 \cdot 10^{-1}$ J, in the halomagnetic field falls in the X-ray region of about $1.6 \cdot 10^{-16}$ to $6.4 \cdot 10^{-14}$ J and should be anisotropic. The synchrotron X rays might be distinguished from X rays produced by other processes, since they would be polarized if the halomagnetic fields were homogeneous on a large scale. The flux of these X rays would be larger from the direction of the galactic center than from the anticenter or the polar regions. Since the diffuse X-ray intensity is roughly isotropic, the synchrotron X-ray contribution should be small.

If an electrically conducting turbulent fluid is acted upon by an approximately homogeneous magnetic field \vec{B}_0 , currents are generated by the induction effect of the turbulent motion and superimpose a perturbation field \vec{B}' on the existing field \vec{B}_0 . The field \vec{B}' induces in the turbulent velocity field \vec{v}' the electromotive forces $\vec{v}' \times \vec{B}'$ whose mean values are generally different from zero, since \vec{B}' is correlated with \vec{v}' . Under conditions which are generally satisfied in rotating turbulent systems, an electromotive force is induced in the direction of \vec{B}_0 . This induction effect of the turbulence maintains the magnetic field.

The conditions in the hydrogen convection zone of the sun are known to some extent; this makes the computation of a solar dynamo possible. Nothing is known about turbulence in the galactic halo. It is probable, however, that it exists, and therefore, the existence of a dynamo in the halo is also probable.

The synchrotron radiation observed at radio frequencies in the galaxy comes from a spheroidal halo (axial ratio 2:1) with a semimajor axis somewhat larger than $3.700 \cdot 10^{20}$ m. The radiation is characterized by little concentration toward the galactic center and toward the galactic plane. No stellar population with such a behavior is known. Therefore, it appears probable that the halo emission originates in a continuous field distribution and not in a large number of unresolved discrete sources. Irregularities in the emission may be due to variations in the magnetic field strength or in the density of the relativistic electrons. The radiation is somewhat stronger near the galactic plane. This additional radiation is usually called the disk component.

The total power emitted by one electron is given by Westfold [25].

$$P(t) = \frac{\mu e^2 c}{6\pi} \frac{\omega^2 \sin^2 \alpha}{\xi^4}$$

$$\xi = \sqrt{1 - \frac{v^2}{c^2}}$$

$$\omega = \frac{e}{m} \sqrt{1 - \frac{v^2}{c^2}} B \quad .$$

For $B = 10^{-9}$ tesla and $f_c = 3 \cdot 10^{-10} \text{ m} \approx 10^{18} \text{ sec}^{-1}$, the relativistic parameter

$$\xi \approx 6.48 \cdot 10^{-9}$$

is required. A single electron would generate the following maximum power density:

$$P(t) \approx 3.78 \cdot 10^{-16} \text{ W m}^{-2}$$

$$F(t) \approx 3.01 \cdot 10^{-17} \text{ W m}^{-2} \text{ sr}^{-1} .$$

The electron density in the galaxy is estimated to have the value:

$$n_e \approx 4 \cdot 10^4 \text{ m}^{-3} .$$

Since the field is estimated to have an extension of at least $3.0856 \cdot 10^{18} \text{ m}$, the required electrons would be easily available.

Summary

After the known X-ray sources in space and their generating processes have been reviewed, a summary of the basic results obtained will be given.

The X-radiation in the sun under nonflare conditions is generated in the corona as deceleration radiation of nonthermal electrons.

The mean magnetic field of the sun is maintained by a dynamo which is activated by turbulence and nonuniform rotation. This field produces no X-radiation. A flare, however, occurs after a short-lived dynamo has been built up. During the first phase of the flare, the dynamo generates microwave, optical, and X-radiation by the synchrotron process. During the second phase of the flare, secondary acceleration occurs because of the collapsing dynamo field whose energy becomes available for this process.

The Crab Nebula emits synchrotron radiation which is maintained by magnetic fields. The only theory which appears to be able to account for the required fields is the dynamo theory. The ex-supernova is surrounded by an extended atmosphere which is in a state of high-energy, turbulent motion. The degrees of magnetization are different for different turbulent elements. The continuum presents a turbulent electromagnetic field, and therefore the conditions for a migratory dynamo exist.

The following stellar X-ray sources have been identified as emitting deceleration (free-free) radiation:

1. Sco X-1.
2. Cyg X-2.
3. Cen X-2.

It has been determined that these three sources have the characteristics of close binary stars and old novae. Assuming that the explosive process has occurred in the nova, a shock wave will penetrate the surface forming an expanded atmosphere in a time which is too short for appreciable loss of radiation. When an electric field exists in a plasma with a density such that the electrons whose velocity surpasses a certain critical value will gain more energy from the field than they lose by collisions, runaway electrons will be generated. Runaway electrons may be the source of deceleration X-radiation in the atmosphere of a nova.

No planetary nebula has been identified as an X-ray source, but a statistical study leads to the conclusion that X-ray sources are more strongly associated with disk Population II objects than with extreme Population I objects. Planetary nebulae emit continuous radiation which originates by free-free transitions involving kinetic energy losses of free electrons in the electrostatic fields of ions. These free-free emissions are responsible for the radiation observed in the radio frequency spectrum. They also contribute in the visible and infrared regions. Therefore, if X rays are generated by planetary nebulae, it can be assumed that they will be produced by free-free transitions, also.

The diffuse background radiation results from the Compton effect where recoil photons are generated by collisions between the universal 3°K distribution and a leakage spectrum of cosmic ray electrons from radio galaxies. Superimposed upon the Compton radiation is synchrotron X-radiation which is produced in a halo dynamo.

FLUID MAGNETIC DYNAMO MODEL OF THE CRAB NEBULA

Introduction

The synchrotron radiation of the Crab Nebula is maintained by magnetic fields. The only theory that appears to be capable of accounting for the required fields is the dynamo theory. For a solution of the dynamo problem, it would be required to solve the fluid-dynamic and electromagnetic equations simultaneously to show that a motion exists which can maintain a given magnetic field and that this motion can be maintained by the forces available. Because of the difficulties of such a complete solution, the more restricted problem is usually treated to consider the motion as assigned and to investigate whether it can maintain a magnetic field. Attempts to consider the dynamo problem in conjunction with the fluid-dynamic equations have been made by Taylor [26] and Gilman [27].

The Crab Nebula

Three type I supernovae and their remnants have been recorded in our galaxy during historical times and are shown in Table 9 [28].

At the levels so far detectable, only the Crab Nebula is an X-ray source. The ex-supernova, a collapsed star, is surrounded by an extended atmosphere which is in a state of high-energy turbulent motion, the degrees of magnetization being different for different turbulent elements. An average of $\approx 10^{31}$ W is injected from the nucleus into the Crab Nebula, which corresponds to $\approx 10^{40}$ relativistic electrons per second. This quantity has to be produced in the nucleus of the nebula.

The Crab Nebula consists of two different parts: a net of thin gaseous filaments arranged in the form of a shell at the periphery of the nebula and a continuous emission which occupies the entire volume of the nebula.

The gaseous shell ejected in the supernova explosion is identical with the system of filaments. The filaments represent sharply defined features, whose emission is concentrated in individual lines. Seen in $H\alpha$, the shell is $3.784 \cdot 10^{16}$ m wide and $5.68 \cdot 10^{16}$ m long. The principal physical parameters describing the conditions in the filaments are:

TABLE 9. THREE TYPE I SUPERNOVAE AND THEIR REMNANTS [28]

Name	Supernovae		
	Crab	Tycho's	Kepler's
Year	1054	1572	1604
l^{II}	184.6	120.1	4.5
b^{II}	-5.8	+1.4	+6.8
m_v (max)	$[-5.5^{\text{m}}]$	-4.0^{m}	-2.2^{m}
Interstellar absorption	1.6^{m}	3.3^{m}	$[2^{\text{m}}]$
Distance ($3.0856 \cdot 10^{16}$ m)	1500	2400	9900
log radio flux at 100 MHz in units of 10^{-26} W m $^{-2}$ (Hz) $^{-1}$	3.25	2.36	1.90
Spectral index	-0.26	-0.61	-0.61
Radio diameters	3'.5 (E.-W. nearly Gaussian)	6' (ring source)	3'.0 (small- scale structure)
log absolute radio luminosity at 100 MHz [10^{-7} W sec $^{-1}$ (Hz) $^{-1}$]	24.68	24.20	24.97
Expansion velocity (km/sec)	1400	5900	12 100

$$R \approx 2.5 \cdot 10^{16} \text{ m}$$

$$N_e \approx 10^9 \text{ m}^{-3}$$

$$M \approx 0.1 M_{\odot}$$

$$T \approx 17\,000 \text{ }^{\circ}\text{K}$$

$$B \approx 3 \cdot 10^{-4} \text{ gauss} = 3 \cdot 10^{-8} \text{ tesla} .$$

These conditions do not apply to the region where the synchrotron radiation is generated. In the continuum, the nebula possesses structure which has no relation to the filaments. The continuum is resolved into fibers. An explanation for the existence and alignment of the fibers is to be found in the confinement of a current filament by its own magnetic field, which is known as the "pinch effect." The cause of the constriction is the electromagnetic attraction between parallel currents. This constriction of currents is accompanied by an accumulation of matter, which explains the fibrous structures.

The filamentary shell encloses a region emitting radiation in the optical continuum, which displays varying degrees of polarization with position. Compared to the mass of the shell, the continuum is negligible, of the order of $10^{-8} M_{\odot}$. The energy spectrum can be expressed as a power law:

$$\frac{dN}{d\epsilon} = K \epsilon^{-\beta}$$

$$\beta = 1 - .2 \alpha .$$

The term α denotes the spectral index, which changes near 10^{14} Hz from about -0.3 at low frequencies to -1.0 at high frequencies. The electron-energy spectrum is therefore roughly $E^{-1.6}$ from $\epsilon \approx 0$ to $\epsilon \approx \epsilon_1$, the energy of particles emitting near 10^{14} Hz, and E^{-3} from ϵ_1 to some upper cutoff energy ϵ_2 .

The X- and γ -ray spectra can be joined smoothly to the optical data. The ultraviolet region of the spectrum has not been observed, but the correct ionization conditions are produced in the filaments if the ultraviolet synchrotron radiation is taken to be an interpolation between the optical and X-ray regions according to the power law. Therefore, the radiation from the Crab Nebula can be considered as a unified synchrotron spectrum that extends from about 10^8 to 10^{20} Hz. Continuous injection of a power-law electron spectrum at a rate proportional to $(\tau - t)^{0.86}$, where τ denotes the age of the nebula approximately, results in a spectrum of the type observed.

Near the center of the nebula are local enhancements of the general synchrotron emission, which are unrelated to the filaments. The features undergo rapid changes. A characteristic configuration, however, recurs and is called a wisp. The wisps emit a continuum which is strongly polarized.

The picture of the continuum can be summarized as follows:

1. The continuum shares the general expansion, demonstrated most clearly by the filaments.
2. Superimposed on this expansion is a field of chaotic motions throughout the nebula, but with a trend toward decreasing velocity with increasing distance from the center.
3. The fastest motions are confined to the central area.

The wisps are also local compressions in the magnetic field. The direction of propagation is perpendicular to the local field direction. Near the center of the nebula, the wisps propagate at about $0.6 \cdot 10^8$ m, damping out after five or six periods. Further from the center, the enhancements propagate at about $0.06 \cdot 10^8$ m. The observed translations of the brightened regions are formed by mass motion, in which the gas and the field move together. The motion is quasi-harmonic, the restoring force being supplied by the magnetic field. The thermal particle density of the main wisp is about:

$$N_{th} \approx 10^3 \text{ m}^{-3} .$$

This number is six orders of magnitude less than the known densities in the filaments. The physical picture is that wisp 1 plays the role of a piston moving back and forth, generating compressional waves which propagate outward.

In the central region of the Crab Nebula, the field lines are generally aligned and parallel to the wisps, although the wisps sometimes curve outward. This is the configuration which might be produced by a small object emitting ionized gas in all directions in an initially uniform magnetic field. The particles emitted perpendicular to the initial field drag the field and plasma outward, leaving behind a hole devoid of field and the original plasma. The interface between the hole and surrounding plasma forms a compressed region, which is identified as wisp 1. Motions result from lack of perfect balance between the outward particle pressure and the inward magnetic pressure. The motions in turn generate compressional waves travelling outward from the center. This model is basically symmetrical, but some departure exists from exact symmetry.

We are looking at a surface of rotation perpendicular to the axis. The power output is presently about:

$$L \approx 7 \cdot 10^{30} \text{ W} .$$

The total energy injected into the nebula in the form of relativistic electrons is:

$$W \approx 5 \cdot 10^{42} \text{ J} .$$

The average magnetic field is:

$$B \approx 3 \cdot 10^{-8} \text{ tesla} .$$

Near the wisps, the Alfvén velocity equals:

$$v_A \approx 3 \cdot 10^7 \text{ m} .$$

The ex-supernova is surrounded by an extended atmosphere which is in a state of high-energy turbulent motion. The degrees of magnetization are different for different turbulent elements. The magnetic field of the nebula is essentially radial between the remnant and the expanding shell. The continuum presents a turbulent electromagnetic field, and therefore, the conditions exist for a migratory dynamo.

The particles injected into the field are preferentially relativistic electrons. The contribution from relativistic protons and heavy nuclei is insignificant.

The radio and optical pulsar NP 0532 is also an X-ray pulsar. It is close to the center of the Crab Nebula and was formed in the supernova explosion of 1054.

Magnetofluid Dynamos

A number of promising dynamo theories have been proposed, almost always with a view to solar application. None of them can be applied to the Crab Nebula numerically yet, since the structure of the Crab Nebula is not known with sufficient accuracy. A survey of the available stellar dynamo models will be given, stressing the basic ideas, not the mathematical application.

Parker's Model. Parker's migratory dynamo is intended to explain the sunspots and some of the solar prominence activity [29]. The generation of a magnetic field \vec{B} by a fluid with velocity \vec{v} and conductivity σ is described by the induction equations:

$$\begin{aligned}\frac{\partial \vec{B}}{\partial t} &= \text{curl} (\vec{v} \times \vec{B}) + \frac{1}{\mu_0 \sigma} \nabla^2 \vec{B} \\ \frac{\partial \vec{A}}{\partial t} &= (\vec{v} \times \vec{B}) - \frac{1}{\mu_0 \sigma} \text{curl} \vec{B} .\end{aligned}\tag{1}$$

By a suitable Cartesian coordinate system and suitable boundary conditions, equation (1) is reduced to the form:

$$\begin{aligned}\frac{\partial B}{\partial t} &= H \frac{\partial A}{\partial x} + \frac{1}{\mu_0 \sigma} \nabla^2 B \\ \frac{\partial A}{\partial t} &= \Gamma B + \frac{1}{\mu_0 \sigma} \nabla^2 A .\end{aligned}\tag{2}$$

The term Γ has the dimension of a velocity and is a measure of the violence of cyclonic fluid motions; Γ and H are assumed to be constants; and equation (1) is reduced to two simultaneous linear equations [eq. (2)] with constant coefficients. Equation (2) is solved by the migratory dynamo waves:

$$\begin{aligned}B &= B_0 e^{i(\omega t + Kx)} \\ A &= A_0 e^{i(\omega t + Kx)} .\end{aligned}\tag{3}$$

In equation (3) ω can be expressed in terms of the constants in equation (2).

Parker uses these waves as explanation for the fact that sunspots appear in low latitudes only, for the migration of the region of formation of sunspots toward the equator, and for the reversal of spot polarity between cycles.

Braginsky's Model [30]. If the magnetic Reynolds number of the fluid is large,

$$1 \ll R_m = \mu_0 \sigma V \ell \quad ,$$

a very weak generation process is sufficient to maintain the magnetic field. According to Cowling's theorem, no generation process exists in the case of axial symmetry; therefore, if $1 \ll R_m$, it is of interest to consider the case of a small deviation from axial symmetry, where a generation process may exist which, although weak, may be sufficient for dynamo operation. At first, the induction equations are expressed for the case where the velocity and magnetic fields have axial symmetry. To separate the axially-symmetrical part of any quantity from the purely variable part, the operation of averaging over the cylindrical coordinate φ is introduced. An equation for the part of \vec{B} variable in φ is obtained by subtracting the inductions averaged over φ from the original induction equations. The attempt is made to obtain a solution of the resulting equation in the form of an expression in powers of R_m^{-1} . The process of field generation is then represented explicitly in the terms for $\frac{\partial \vec{B}}{\partial t}$ and $\frac{\partial \vec{A}}{\partial t}$. In the case of inhomogeneous rotation, the second terms can be interpreted as the drawing out of the magnetic field lines from the meridional field in the azimuthal direction, and the azimuthal electromagnetic force generates a meridional from the azimuthal field.

Taylor's Model. Although Taylor applied the self-excited dynamo to the earth, it may also be applicable to the Crab Nebula. Taylor's model uses, in addition to the induction equation (1), the equations of fluid dynamics in the form:

$$\begin{aligned} 2\rho (\vec{\omega} \times \vec{v}) &= (\vec{J} \times \vec{B}) - \nabla p \\ \text{div } \vec{v} &= 0 \\ \frac{\partial \rho}{\partial t} &= -(\vec{v} \cdot \nabla) \rho \quad . \end{aligned} \tag{4}$$

To solve these equations, Taylor proves the following theorem: If the rotating fluid is contained in a rigid envelope in the form of a surface of revolution, then a velocity \vec{v} compatible with the equations (1) and (4) will

exist if and only if the magnetic field satisfies the following constraint, expressed in cylindrical coordinates (r, φ, z) :

$$\int_{r=\text{const}} (\vec{J} \times \vec{B})_{\varphi} d\varphi dz = 0 \quad . \quad (5)$$

To show that equation (5) is necessary, the φ -component of the first part of equation (4) is integrated over that part of the cylinder which lies within the fluid, considered to be enclosed in a sphere, but the proof applies to any surface of revolution. The integrand on the left-hand side is expanded, and finally transformed according to Gauss's theorem. The necessity of the condition follows then from the second part of equation (4).

The proof that equation (5) is sufficient is given by providing an algorithm for the determination of \vec{v} in terms of \vec{B} and ρ . If equation (5) is to be sufficient, it has to be shown that the first two parts of equation (4), together with the boundary condition,

$$(\vec{v} \cdot \vec{n}) = 0 \quad ,$$

on the surface of the sphere, determine \vec{v} if \vec{B} and ρ are given.

Equation (5) expresses the fact that the moment exerted by the magnetic forces on any cylinder of fluid, coaxial with the axis of rotation must vanish. If equation (5) is satisfied, the instantaneous fluid velocity is specified by the instantaneous values of \vec{B} and ρ , together with the boundary conditions of vanishing normal velocity over a sphere, or other surface of revolution satisfying the conditions of the theorem, except for an azimuthal velocity $u_{\phi}(r)$.

This azimuthal velocity is determined by the requirement that equation (5) continues to be satisfied as \vec{B} develops according to the electromagnetic equation (1).

Gilman's Model. A Rossby wave is defined to be a nearly, but not entirely, horizontal wavy or eddying flow pattern in a rotating fluid in which Coriolis forces nearly balance horizontal pressure forces. It is assumed that a latitudinal gradient large enough to excite Rossby waves exists in the convection zone of the sun, and the fluid magnetic effects of the waves are examined. It is also assumed that the Rossby number is small:

$$R_o = \frac{V}{2\Omega l} \ll 1 \quad .$$

The basic equations of magnetofluid dynamics are introduced in dimensionless variables. The equations are the horizontal and vertical equations of motion, the equation of continuity, the horizontal and vertical magnetic field induction equations, the magnetic field continuity equation, and the heat conduction equation. The dependent variables (pressure, density, specific volume, and temperature) expressed in power series in terms of R_0 are assumed to be small. If K denotes any of the variables, it is expanded in the form:

$$K = K^{(0)} + R_0 K^{(1)} + R_0^2 K^{(2)} + O(R_0^3)$$

and substituted into the equations of fluid-dynamics. Collecting first-order terms, it is noticed from the horizontal magnetic field induction equation, which is the prediction equation for the toroidal field, that it contains two terms representing the stretching of poloidal into toroidal fields. From the first-order terms of the vertical field induction equations, and including a second-order term, the induction of the poloidal field from the toroidal field — accomplished by the vertical motion twisting toroidal field lines up into the vertical — is obtained.

Four first-order and one second-order equations form the equations for the dynamo. As in Taylor's dynamo, the motion is not given but is generated by latitudinally nonuniform heating. The induced magnetic fields react upon the inducing motions. Therefore, a state of balance should be reached in which, on the average, induction of new fields is balanced by dissipation.

The Steenbeck and Krause Model. Currently, the Steenbeck and Krause model offers the best developed procedure to obtain magnetic fields [31]. In this model, Parker's [29] and Braginsky's [30] ideas are utilized and expanded such that computer application becomes possible. It is concerned with the restricted problem in which \vec{v} is considered as given. If a model of the Crab Nebula were known, with a precision comparable to that of solar models, the structure of the magnetic field of the Crab Nebula could be computed.

The first part of equation (1) and the second part of equation (2) are used and expressed in spherical coordinates. The terms A and B are developed into a series of Legendre polynomials. By considering the relations existing between Legendre functions, an infinite system of ordinary differential equations is obtained. This system decomposes into two uncoupled systems, and the problem to find nontrivial solutions for the two systems that are regular at the origin and satisfy the boundary conditions at the surface leads to a two-parameter

characteristic value problem for two characteristic values. This problem for an infinite system of ordinary differential equations is solved in such a way that it is broken off at a particular value N . The remaining finite system is solved. To test the convergence, N is increased step by step until the characteristic values are unchanged within the required accuracy. The integration of the system of differential equations is performed in accordance with the Runge-Kutta procedure. The solution of the characteristic value problem is performed with an electronic computer.

The Bouncing Core Theory of the Crab's Pulsar

It was shown by Harrison [32] that the principal properties of pulsars can be explained if the falling core of a collapsing star rebounds at finite or infinite density as assumed in the oscillating model of the universe. The condition that the metric remains nonsingular — with the exception of the infinite density bounce — can be satisfied. The intermediate configurations then become pulsating structures, for which the rise and fall of the core is the regulating principle. In the rising phase, the core and its adjacent shells emit intense blueshifted radiation. The periodic emission and the accurate timing of pulsars are explained by the theory that catastrophic collapse results in a bouncing-core structure, the outer layers of which are supported by periodic radiation from the core.

The observed pulsed emissions originate from the underlying layers, which participate in the motion of the core but oscillate with limited amplitude. The pulse of enhanced radiation emitted during the rising phase is seen by a distant observer to be contracted in time. Between pulses, the radiation is reduced and the time is dilated. This is because the observed pulse is short compared with the period. Radiation from underlying shells adjacent to the core will also augment the pulse, but this radiation will cease between pulses.

Energy is radiated at the expense of increasing the binding energy of the original core mass at infinite dispersion. In the bouncing-core theory of pulsars, the period is regulated by gravitational collapse and expansion. The observed period is increased by redshift. The central region has no equilibrium configuration. The pulse originates as a burst of radiation from shells adjacent to the core during expansion. Its observed width is contracted because of the predominating Doppler effect. Pulsed emission is an essential characteristic of bouncing-core configurations. The energy is gravitational in origin. Loss of energy causes the ceiling radius of the core to shrink towards the

Schwarzschild radius and increases the period. The pulsars observed so far are approaching the end point of stellar evolution and are expending the last remnants of available energy.

For NP 0532 in the Crab, for $1M_{\odot}$, the rate at which energy escapes according to the theory is $6 \cdot 10^{31}$ W, in rough agreement with the energy requirements of the nebula.

Most supernovae are possibly poorly-clad bouncing cores and are therefore short-lived pulsars relasing energy rapidly.

To obtain nonstationary solutions of general relativity, the following assumptions are made:

1. The field equations are valid in their most general form, containing the cosmological constant:

$$R_{ik} - 1/2 g_{ik} R + \lambda g_{ik} = -K T_{ik} \quad (6)$$

2. The velocity of matter is negligible in comparison with the velocity of light. Then the momentum-energy tensor is given by:

$$T_{ik} = 0, \text{ if } i, k \neq 4$$

$$T_{44} = c^2 \rho g_{44} \quad .$$

3. The metric is given in the form:

$$ds^2 = R^2 (dx^1{}^2 + \sin^2 x^1 dx^2{}^2 + \sin^2 x^1 \sin^2 x^2 dx^3{}^2) + M^2 dx^4{}^2$$

with R and M depending on x^4 . By a suitable choice of x^4 , the condition

$$M = 1$$

can be satisfied without loss of generality. The metric can be brought into the form:

$$d\tau^2 = - \frac{1}{c^2} ds^2$$

$$d\tau^2 = - \frac{[R(x^4)]^2}{c^2} (dx^1{}^2 + \sin^2 x^1 dx^2{}^2 + \sin^2 x^1 \sin^2 x^2 dx^3{}^2) + dx^4{}^2 \quad .$$

The terms R and ρ are to be determined from the field equations. For $i = k = 1, 2, 3$, equation (6) yields a relation:

$$\frac{R^1}{R^2} + \frac{2RR^{11}}{R^2} + \frac{c^2}{R^2} - \lambda = 0 \quad . \quad (7)$$

The integration of equation (7), writing t for x^4 , yields the following equation:

$$\frac{1}{c^2} \left(\frac{dR}{dt} \right)^2 = \frac{A - R + \frac{\lambda}{3c^2} R^3}{R} \quad . \quad (8)$$

The integration constant is denoted by A . From this equation, R is obtained by inversion of an elliptical integral, i. e., by solving the equation:

$$t = \frac{1}{c} \int \frac{R}{\sqrt{A - x + \frac{\lambda}{3c^2} x^3}} dx + B \quad (9)$$

with respect to R . Constants are denoted by B and A . For the nonstationary solutions, equations (8) and (9) have to be considered. The term λ remains undetermined; it is assumed that λ can take arbitrary values but lies in the interval $\left(-\infty, \frac{4c^2}{9A^2} \right)$. In that case, R becomes a periodic function of t , with the period $t_\pi \cdot t_\pi$ given by the formula:

$$t_\pi = \frac{2}{c} \int_0^{x_0} \sqrt{\frac{x}{A - x + \frac{\lambda}{3c^2} x^3}} dx \quad .$$

The term x_0 is a function of λ and A :

$$x_0 = \Theta(\lambda, A) \quad .$$

The radius of curvature varies between 0 and x_0 . This is called the periodic solution. For small λ , the period is represented by the approximate formula:

$$t_\pi = \frac{\pi A}{c} \quad .$$

REFERENCES

1. Fujimoto, M. ; Hayakawa, S. ; and Kato, T. : Correlation Between the Densities of X-Ray Sources and Interstellar Gas. *Astrophys. and Space Sci.*, Vol. 4, 1969, pp. 64-83.
2. Friedman, H. ; Byram, E. T. ; and Chubb, T. A. : Distribution and Variability of Cosmic X-Ray Sources. *Science*, Vol. 156, 1967, pp. 374-378.
3. Landolt-Boernstein: *Astronomy and Astrophysics*, Vol. 1, Group 6, Springer, Heidelberg-New York, 1965.
4. Kopal, Z. : *Close Binary Systems*. John Wiley & Sons, Inc., New York, 1959.
5. Matsuoka, M. ; Oda, M. ; Ogawara, Y. ; Hayakawa, S. ; and Kato, T. : Measurement of the Absolute Intensity of Cosmic X-Rays. *Astrophys. and Space Sci.*, Vol. 4, 1969, pp. 44-63.
6. Felten, J. E. ; and Gould, R. J. : Interstellar and Intergalactic Absorption of Cosmic X Rays. *Phys. Rev. Letters*, Vol. 17, 1966, pp. 401-405.
7. Rao, U. R. ; Chitnis, E. V. ; Prakasarao, A. T. ; and Jayanthi, U. B. : X-Ray Flux from Centaurus X-2 in the Energy Range 2-20 keV. *Astrophys. J.*, Vol. 157, 1968, pp. L127-L132.
8. Grader, R. J. ; Hill, R. W. ; Seward, F. D. ; and Toor, A. : X-Ray Spectra from Three Cosmic Sources. *Science*, Vol. 152, 1966, pp. 1499-1504.
9. Cooke, B. ; Pounds, K. ; Stewardson, E. ; and Adams, D. : A Cosmic Ray Survey in the Southern Hemisphere. *Astrophys. J.*, Vol. 150, 1967, pp. L189-L191.
10. Chodil, G. ; Mark, H. ; Rodrigues, R. ; Seward, F. ; Swift, C. D. ; Hiltner, W. A. ; Walerstein, G. ; and Mannery, E. J. : Spectral and Location Measurements of Several Cosmic X-Ray Sources Including a Variable Source in Centaurus. *Phys. Rev. Letters*, Vol. 19, 1967, pp. 681-683.

REFERENCES (Continued)

11. Chodil, G. ; Mark, H. ; Rodrigues, R. ; Seward, F. D. ; Swift, C. D. ; Turiel, I. ; Hiltner, W. A. ; Wallerstein, G. ; and Mannery, E. J. : Simultaneous Observations of the Optical and X-Ray Spectra of Sco XR-1. *Astrophys. J.*, Vol. 154, 1968, pp. 645-654.
12. Lewin, W. H. G. ; Clark, G. W. ; and Smith, W. B. : Observation of an X-Ray Flare from Xco X-1. *Astrophys. J.*, Vol. 152, 1968, pp. L155-L161.
13. Deupree, R. : Statistical Correlations of Position Between X-Ray Sources and Optical Objects. *Pub. Astn. Soc. Pac.*, Vol. 81, 1969, pp. 130-133.
14. Wheeler, J. A. : Superdense Stars. *Ann. Rev. Astrophys.*, Vol. 4, 1966, pp. 393-432.
15. Shklovsky, I. S. : Supernovae. John Wiley & Sons, Inc., London-New York-Sydney, 1968.
16. Plavec, M. : Mass Exchange and Evolution of Close Binaries. *Adv. in Astron. Astrophys.*, Vol. 6, 1968, pp. 201-278.
17. Woltjer, L. : Galactic Magnetic Fields. *The Structure and Evolution of Galaxies*. Institute Sobvay, Interscience Publ., London-New York-Sydney, 1965, pp. 30-45.
18. Woltjer, L. : Dynamics of Gas and Magnetic Fields, Spiral Structure. *Galactic Structure*. (ed. A. Blaauw and M. Schmidt), U. of Chicago Press, Chicago, 1965, pp. 531-587.
19. Gorenstein, P. ; Kellogg, E. M. ; and Gursky, H. : The Spectrum of Diffuse Cosmic X-Rays, 1-13 keV. *Astrophys J.*, Vol. 156, 1969, pp. 315-324.
20. Bleeker, A. M. ; and Deerenberg, A. J. M. : The Diffuse Cosmic X-Ray Background from 20 to 220 keV. *Astrophys. J.*, Vol. 159, 1970, pp. 215-228.

REFERENCES (Concluded)

21. Brown, R. L.: Production of the Diffuse Background X-Ray Flux at 44 Å by Superthermal Proton Bremsstrahlung. *Astrophys. J.*, Vol. 159, 1970, pp. L187-L192.
22. Clark, G. W.: The Relation Between Cosmic γ -Rays and Synchrotron X-Rays. *Nuovo Cimento*, Vol. 30, 1963, pp. 727-733.
23. Ginzburg, V. L.; and Syrovatsky, S. I.: Some Problems in Gamma- and X-Ray Astronomy. *Space Sci. Rev.*, Vol. 4, 1965, pp. 267-312.
24. Verma, S. D.: High Energy Electrons and Emission of the Omnidirectional Synchrotron Radiation in Radio-Frequency and X-Ray Regions. *Astrophys. J.*, Vol. 152, 1968, pp. 537-544.
25. Westfold, K. C.: The Polarization of Synchrotron Radiation. *Astrophys. J.*, Vol. 130, 1959, pp. 241-258.
26. Taylor, J. B.: The Magneto-Hydrodynamics of a Rotating Fluid and the Earth's Dynamo Problem. *Proc. Roy. Soc. London A.*, Vol. 274, 1963, pp. 274-283.
27. Gilman, P. A.: A Rossby-Wave Dynamo for the Sun I. *Solar Physics*, Vol. 8, 1969, pp. 316-330.
28. Woltjer, L.: X-Rays and Type I Supernova Remnants. *Astrophys. J.*, Vol. 140, 1964, pp. 1309-1313.
29. Parker, E. N.: Hydromagnetic Dynamo Models. *Astrophys. J.*, Vol. 122, 1955, pp. 293-314.
30. Braginsky, S. I.: Self-Excitation of a Magnetic Field During the Motion of a Highly Conducting Fluid. *Soviet Physics JETP*, Vol. 20, 1965, pp. 726-735.
31. Steenbeck, M.; and Krause, F.: Zur Dynamo Theorie Stellarer and Planetarer Magnetfelder. I. *Astr. Nachr.*, Vol. 291, 1969, pp. 49-84.
32. Harrison, E. R.: Bouncing Core Theory of Pulsars. *Nature*, Vol. 225, 1970, pp. 44-46.

BIBLIOGRAPHY

- Bleeker, J. A. M.; and Deerenberg, A. J. M.: The Diffuse Cosmic X-Ray, Background from 20 to 220 keV. *Astrophys. J.*, Vol. 154, 1970, pp. 215-228.
- Brecher, K.; and Morrison, P.: Cosmology, Black-Body Radiation, and the Diffuse X-Ray Background. *Astrophys. J.*, Vol. 150, 1967, pp. L61-L64.
- Cooke, B. A.; Pounds, K. A.; and Stewardson, E. A.: A Cosmic X-Ray Survey in the Southern Hemisphere. *Highlights of Astronomy*. (ed. L. Perek), 1968, pp. 188-191.
- Editorial: Further Observations of Pulsars. *Sky and Telescope*, Vol. 37, 1969, p. 366.
- Eggen, O. J.; Freeman, K. C.; and Sandage, A.: On the Optical Identification of the X-Ray Source Cen XR-2 as WX Cen. *Astrophys. J.*, Vol. 154, 1968, pp. L27-L31.
- Felton, E.; and Morrison, P.: Omnidirectional Inverse Compton and Synchrotron Radiation from Cosmic Distributions of Fast Electrons and Thermal Photons. *Astrophys. J.*, Vol. 146, 1966, pp. 686-708.
- Fishman, G. J.; Harnden, F. R.; and Haymes, R. C.: Observation of Pulsed Hard X-Radiation from NP 0532 from 1967 Data. *Astrophys. J.*, Vol. 156, 1969, pp. L107-L110.
- Friedman, A.: Ueber die Krümmung des Raumes. *Zs. f. Phys.*, Vol. 10, 1922, pp. 377-386.
- Friedman, H. M.: X Rays from Stars and Nebulae. *Ann. Rev. Nucl. Sci.*, Vol. 17, 1967, pp. 317-346.
- Fritz, G.; Henry, R. C.; Meekins, J. F.; Chubb, T. A.; and Friedman, H.: X-Ray Pulsar in the Crab Nebula. *Science*, Vol. 164, 1969, pp. 709-712.
- Fritz, G.; Meekins, J. F.; Henry, R. C.; Byram, E. T.; and Friedman, H.: Soft X Rays from Scorpius XR-1. *Astrophys. J.*, Vol. 153, 1968, pp. L199-L202.

BIBLIOGRAPHY (Continued)

- Gorenstein, P. ; Giacconi, R. ; and Gursky, H. : The Spectra of Several X-Ray Sources in Cygnus and Scorpio. *Astrophys. J.*, Vol. 150, 1967, pp. L85-L94.
- Gorenstein, P. ; Gursky, H. ; and Garmire, G. : The Analysis of X-Ray Spectra. *Astrophys. J.*, Vol. 153, 1968, pp. 885-897.
- Gorenstein, P. , Kellogg, E. M. ; and Gursky, H. : The Spectrum of Diffuse Cosmic X-Rays, 1-13 keV. *Astrophys. J.*, Vol. 156, 1969, pp. 315-324.
- Grader, R. J. ; Hill, R. W. ; Seward, F. D. ; and Hiltner, W. A. : The Soft X-Ray Spectra of Three Cosmic Sources and Simultaneous Optical Observations of Sco XR-1. *Astrophys. J.*, Vol. 159, 1970, pp. 201-214.
- Green, L. C. : Pulsars. *Sky and Telescope*, Vol. 37, 1969, pp. 214-218.
- Gursky, H. ; Gorenstein, P. ; and Giacconi, R. : The Distribution of Galactic X-Ray Sources from Scorpio to Cygnus. *Astrophys. J.*, Vol. 150, 1967, pp. L75-L84.
- Haymes, R. C. ; Ellis, D. V. ; Fishman, G. J. ; Kurfess, J. D. ; and Tucker, W. H. : Observation of γ -Radiation from the Crab Nebula. *Astrophys. J.*, Vol. 151, 1968, pp. L9-L14.
- Haymes, R. C. ; and Craddock, W. L. : High-Energy X-Rays from the Crab Nebula. *J. Geophys. Res.*, Vol. 71, 1966, pp. 3261-3264.
- Hill, R. W. ; Grader, R. J. ; and Seward, F. D. : The Soft X-Ray Spectrum of Sco XR-1. *Astrophys. J.*, Vol. 154, 1968, pp. 655-660.
- Johnson, H. M. : Physical Characteristics of Sco X-1. *Astrophys. J.*, Vol. 146, 1966, pp. 960-961.
- Johnson, H. M. : Physical Characteristics of Sco X-1. *Astrophys. J.*, Vol. 154, 1968, pp. 1139-1141.
- Kraft, R. P. ; and Demoulin, M. H. : On the Remarkable Spectroscopic Complexities of Cyg X-2. *Astrophys. J.*, Vol. 150, 1967, pp. L183-L188.

BIBLIOGRAPHY (Continued)

- Kraft, R. P. ; and Miller, J. S. : Further Spectroscopic Observations of the Optical Object Identified with X-Ray Source Cygnus X-2. *Astrophys. J.* , Vol. 155, 1969, pp. L159-L161.
- Kristian, J. ; Sandage, A. ; and Westphal, J. A. : Rapid Photometric and Spectroscopic Variations of the X-Ray Source Cyg X-2. *Astrophys. J.* , Vol. 150, 1967, pp. L99-L105.
- Melrose, P. B. : Acceleration of Ultrarelativistic Electrons in the Crab Nebula. *Astrophys. and Space Sci.* , Vol. 4, 1969, pp. 165-181.
- Morrison, P. : Extrasolar X-Ray Sources. *Ann. Rev. Astron. Astrophys.* , Vol. 5, 1967, pp. 325-350.
- Neugebauer, G. ; Oke, J. B. ; Becklin, E. ; and Garmire, G. : A Study of Visual and Infrared Observations of Sco XR-1. *Astrophys. J.* , Vol. 155, 1969, pp. 1-9.
- Overbeck W. ; and Tananbaum, H. D. : Time Variations in Scorpius X-1 and Cygnus XR-1. *Astrophys. J.* , Vol. 153, 1968, pp. 899-908.
- Parker, E. N. : The Generation of Magnetic Fields in Astrophysical Bodies. *Astrophys. J.* , Vol. 162, 1970, pp. 665-673.
- Parker, E. N. : The Generation of Magnetic Fields in Astrophysical Bodies. *Astrophys. J.* , Vol. 163, 1971, pp. 255-285.
- Prendergast, K. H. ; and Burbidge, G. R. : On the Nature of Some Galactic X-Ray Sources. *Astrophys. J.* , Vol. 151, 1968, pp. L83-L88.
- Roxburgh, I. W. : On the Fission Theory of the Origin of Binary Stars. *Astrophys. J.* , Vol. 143, 1969, pp. 11-120.
- Scargle, J. D. : Activity in the Crab Nebula. *Astrophys. J.* , Vol. 156, 1969, pp. 401-426.
- Scheuer, P. A. G. : Radiation. *Proc. Intern. School of Physics "Enrico Fermi,"* Vol. 39, 1967, pp. 289-306.
- Shklovsky, I. : Concerning the Nature of the Sky Background of Soft X-Ray Emission. *Astrophys. Letters* , Vol. 3, 1969, pp. 1-2.

BIBLIOGRAPHY (Concluded)

- Sommerfeld, A.: *Electrodynamics*. Academic Press, New York-London, 1964.
- van den Bergh, S.; and Dodd, W. W.: Search for an Optical Remnant of the Cassiopeia A Supernova. *Nature*, Vol. 223, 1969, pp. 814-815.
- van Genderen, A. M.: 5-Color Photometry of the X-Ray Source Sco X-1. *Astron. and Astrophys.*, Vol. 2, 1969, pp. 6-17.
- Wallerstein, G.: On the Distance to the Star Associated with Scorpio XR-1. *Astrophys. Letters*, Vol. 1, 1967, pp. 31-32.
- Wilson, R. E.; and Sofia, S.: Model of Cygnus X-2. *Nature*, Vol. 223, 1969, pp. 1350-1351.

APPROVAL

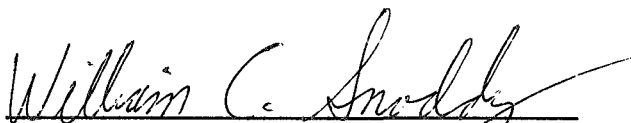
TM X-64571

CONTRIBUTIONS TO X-RAY PHYSICS IN SPACE

By Klaus Schocken

The information in this report has been reviewed for security classification. Review of any information concerning Department of Defense or Atomic Energy Commission programs has been made by the MSFC Security Classification Officer. This report, in its entirety, has been determined to be unclassified.

This document has also been reviewed and approved for technical accuracy.



WILLIAM C. SNODDY
Chief, Space Thermophysics Division



GERHARD B. HELLER
Director, Space Sciences Laboratory

DISTRIBUTION

INTERNAL

DIR

AD-S

Dr. Ernst Stuhlinger

S&E-DIR

Mr. Hermann Weidner

S&E-R

Dr. William Johnson

PD-MP

Mr. James Downey

S&E-AERO-T

Dr. Helmut Krause

S&E-SSL-DIR

Mr. Gerhard Heller

Mr. Ray Hembree

S&E-SSL-X

Dr. James B. Dozier

Mr. Hoyt Weathers

S&E-SSL-C

Mr. Billy Bass

Reserve (15)

S&E-SSL-N

Dr. Rudolf Decher

S&E-SSL-S

Dr. Werner Sieber

S&E-SSL-P

Dr. Robert Naumann

S&E-SSL-T

Mr. William Snoddy

Dr. Klaus Schocken (10)

S&E-SSL-TE

Mr. Ed Miller

Mr. Harry Atkins

Mr. Walter Fountain

Mr. James Fountain

Mr. Stanley Fields

Mr. John Reynolds

Mr. Charles Baugher

Mr. Ed Reichmann

Mr. Robert Wilson

S&E-SSL-TT

Mr. Billy Jones

Mr. Daniel Gates

Mr. Paul Craven

Mr. Jimmy Watkins

Dr. Mona J. Hagyard

Mr. Ted Calvert

Dr. Gilmer Gary

S&E-SSL-TR

Mr. Gary Arnett

Mr. Tommy Bannister

Dr. Roger Kroes

Mr. Roger Linton

Mr. Donald Wilkes

Mr. James Zwiener

Miss Barbara Richard

Dr. Ulrich Wegner

Dr. Kulshreshtha

DEP-T

A&TS-PAT

Mr. L. D. Wofford, Jr.

DISTRIBUTION (Concluded)

INTERNAL (Concluded)

PM-PR-M
A&TS-MS-IP (2)
A&TS-MS-IL (8)
A&TS-TU (6)
A&TS-MS-H

EXTERNAL

National Aeronautics and Space Administration
Washington, D. C. 20546

Attn: Dr. A. Boggess, Code 613
Dr. K. Hallan, Code 613
Dr. T. Stecher, Code 613
Dr. J. Underwood, Code 614
Dr. E. Boldt, Code 611

Manned Spacecraft Center
Houston, Texas 77058
Attn: Dr. Yoji Kondo, TG4

Scientific and Technical Information Facility (25)
P. O. Box 33
College Park, Maryland 20740
Attn: NASA Representative (S-AK/RKT)

Dr. Edward J. Devinney
Department of Astronomy
University of South Florida
Tampa, Florida 33620

Dr. Laurence E. Peterson
Department of Physics
Space Physics Group
University of California
La Jolla, California 92037